ELECTROCHEMISTRY RESEARCH LABORATORY

DEPARTMENT OF CHEMISTRY
JOHN SCHOFF MILLIS SCIENCE CENTER
CASE WESTERN RESERVE UNIVERSITY
CLEVELAND, OHIO 44106

TECHNICAL REPORT NO. 30

DIFFERENTIAL CAPACITANCE STUDY ON THE BASAL PLANE OF STRESS-ANNEALED PYROLYTIC GRAPHITE

by

Jean-Paul Randin and Ernest Yeager

15 July 1971

OFFICE OF NAVAL RESEARCH

Contract N00014-67-A-0404-0006

Project NR 359-451

55

R

OFFICE OF NAVAL RESEARCH

Contract N00014-67-A-0404-0006

Project NR 359-451

TECHNICAL REPORT NO. 30

DIFFERENTIAL CAPACITANCE STUDY ON THE BASAL PLANE OF STRESS-ANNEALED PYROLYTIC GRAPHITE

by

Jean-Paul Randin and Ernest Yeager

Department of Chemistry
CASE WESTERN RESERVE UNIVERSITY
Cleveland, Ohio 44106

15 July 1971

DOCUMENT CONTROL DATA · R&D

(Security classification of title, body of abstract and indexing annotation must be entered when the overall report is classified)

1 ORIGINATING ACTIVITY (Corporate author) Case Western Reserve University Cleveland, Ohio 44106, USA	2a REPORT SECURITY CLASSIFICATION Unclassified 2b GROUP ---

3 REPORT TITLE

Differential Capacitance Study on the Basal Plane of Stress-Annealed Pyrolytic Graphite

4 DESCRIPTIVE NOTES (Type of report and inclusive dates)
Technical Report No. 30

5 AUTHOR(S) (Last name, first name, initial)
Randin, Jean-Paul
Yeager, Ernest B.

6 REPORT DATE	7a TOTAL NO. OF PAGES	7b NO. OF REFS
15 July 1971	53	20

8a CONTRACT OR GRANT NO. N00014-67-A-0404-0006 b PROJECT NO. NR 359-451 c. d	9a ORIGINATOR'S REPORT NUMBER(S) Technical Report No. 30 9b OTHER REPORT NO(S) (Any other numbers that may be assigned this report) ----

10 AVAILABILITY/LIMITATION NOTICES
This document has been approved for public release and sale; its distribution is unlimited.

11 SUPPLEMENTARY NOTES	12 SPONSORING MILITARY ACTIVITY
---	Office of Naval Research Arlington, Virginia 22217 Code 472, Chemistry Program

13 ABSTRACT

The non-faradaic differential electrode capacity of the basal plane of high-pressure stress-annealed pyrolytic graphite has been examined in aqueous solution using an a.c. impedance bridge. The capacity has a near parabolic dependence on electrode potential with a minimum of $\sim 3\ \mu f/cm^2$ in concentrated electrolytes and is pH independent. Studies in NaF solutions at concentrations in the range 0.9 to 10^{-5} M indicate that in the range of potential studied (+0.5 to -0.5 V vs NHE) the minimum capacity is best attributed to the space charge region within the graphite and not to the diffuse ionic layer. Apparently the potential of zero charge of the electrolyte is outside the potential range of the measurements.

The capacity value on the basal plane of the stress-annealed pyrolytic graphite compares favorably with that estimated from the carrier concentration using the presently available theory of the space charge layer in semiconductor electrodes.

14 KEY WORDS	LINK A		LINK B		LINK C	
	ROLE	WT	ROLE	WT	ROLE	WT
graphite stress-annealed pyrolytic graphite electrochemistry interface capacity a.c. impedance semi conductor properties basal plane of graphite linear sweep voltammetry current distribution of electrodes						

INSTRUCTIONS

1. ORIGINATING ACTIVITY: Enter the name and address of the contractor, subcontractor, grantee, Department of Defense activity or other organization *(corporate author)* issuing the report.

2*a*. REPORT SECURITY CLASSIFICATION: Enter the overall security classification of the report. Indicate whether "Restricted Data" is included. Marking is to be in accordance with appropriate security regulations.

2*b*. GROUP: Automatic downgrading is specified in DoD Directive 5200.10 and Armed Forces Industrial Manual. Enter the group number. Also, when applicable, show that optional markings have been used for Group 3 and Group 4 as authorized.

3. REPORT TITLE: Enter the complete report title in all capital letters. Titles in all cases should be unclassified. If a meaningful title cannot be selected without classification, show title classification in all capitals in parenthesis immediately following the title.

4. DESCRIPTIVE NOTES: If appropriate, enter the type of report, e.g., interim, progress, summary, annual, or final. Give the inclusive dates when a specific reporting period is covered.

5. AUTHOR(S): Enter the name(s) of author(s) as shown on or in the report. Enter last name, first name, middle initial. If military, show rank and branch of service. The name of the principal author is an absolute minimum requirement.

6. REPORT DATE: Enter the date of the report as day, month, year; or month, year. If more than one date appears on the report, use date of publication.

7*a*. TOTAL NUMBER OF PAGES: The total page count should follow normal pagination procedures, i.e., enter the number of pages containing information.

7*b*. NUMBER OF REFERENCES: Enter the total number of references cited in the report.

8*a*. CONTRACT OR GRANT NUMBER: If appropriate, enter the applicable number of the contract or grant under which the report was written.

8*b*, 8*c*, & 8*d*. PROJECT NUMBER: Enter the appropriate military department identification, such as project number, subproject number, system numbers, task number, etc.

9*a*. ORIGINATOR'S REPORT NUMBER(S): Enter the official report number by which the document will be identified and controlled by the originating activity. This number must be unique to this report.

9*b*. OTHER REPORT NUMBER(S): If the report has been assigned any other report numbers *(either by the originator or by the sponsor)*, also enter this number(s).

10. AVAILABILITY/LIMITATION NOTICES: Enter any limitations on further dissemination of the report, other than those imposed by security classification, using standard statements such as:

(1) "Qualified requesters may obtain copies of this report from DDC."

(2) "Foreign announcement and dissemination of this report by DDC is not authorized."

(3) "U. S. Government agencies may obtain copies of this report directly from DDC. Other qualified DDC users shall request through _____."

(4) "U. S. military agencies may obtain copies of this report directly from DDC. Other qualified users shall request through _____."

(5) "All distribution of this report is controlled. Qualified DDC users shall request through _____."

If the report has been furnished to the Office of Technical Services, Department of Commerce, for sale to the public, indicate this fact and enter the price, if known.

11. SUPPLEMENTARY NOTES: Use for additional explanatory notes.

12. SPONSORING MILITARY ACTIVITY: Enter the name of the departmental project office or laboratory sponsoring *(paying for)* the research and development. Include address.

13. ABSTRACT: Enter an abstract giving a brief and factual summary of the document indicative of the report, even though it may also appear elsewhere in the body of the technical report. If additional space is required, a continuation sheet shall be attached.

It is highly desirable that the abstract of classified reports be unclassified. Each paragraph of the abstract shall end with an indication of the military security classification of the information in the paragraph, represented as *(TS)*, *(S)*, *(C)*, or *(U)*

There is no limitation on the length of the abstract. However, the suggested length is from 150 to 225 words.

14. KEY WORDS: Key words are technically meaningful terms or short phrases that characterize a report and may be used as index entries for cataloging the report. Key words must be selected so that no security classification is required. Identifiers, such as equipment model designation, trade name, military project code name, geographic location, may be used as key words but will be followed by an indication of technical context. The assignment of links, rules, and weights is optional

TABLE OF CONTENTS

DIFFERENTIAL CAPACITANCE STUDY ON THE BASAL PLANE OF STRESS-ANNEALED PYROLYTIC GRAPHITE

by

Jean-Paul Randin* and Ernest Yeager

Chemistry Department
Case Western Reserve University
Cleveland, Ohio 44106

ABSTRACT

The non-faradaic differential electrode capacity of the basal plane of high-pressure stress-annealed pyrolytic graphite has been examined in aqueous solution using an a.c. impedance bridge. The capacity has a near parabolic dependence on electrode potential with a minimum of $\sim 3\ \mu f/cm^2$ in concentrated electrolytes and is pH independent. Studies in NaF solutions at concentrations in the range 0.9 to 10^{-5} M indicate that in the range of potential studied (+0.5 to -0.5 V vs NHE) the minimum capacity is best attributed to the space charge region within the graphite and not to the diffuse ionic layer. Apparently the potential of zero charge of the electrolyte is outside the potential range of the measurements.

The capacity value on the basal plane of the stress-annealed pyrolytic graphite compares favorably with that estimated from the carrier concentration using the presently available theory of the space charge layer in semiconductor electrodes.

---

*Present address: Hydro-Quebec Institute of Research, Varennes, Quebec, CANADA

In a previous note (1), the non-faradaic differential capacitv measured on the basal plane of stress-annealed pvrolvtic graphite has been reported to have a near parabolic dependence on electrode potential with a minimum of about 3 $\mu f/cm^2$ in 0.9 N NaF. This surprisingly low capacity value was explained on the basis that a substantial fraction of the potential change between the electrode and the solution occurs across a space charge layer within the graphite.

In the present study, further a.c. impedance measurements and linear sweep voltammetry are reported on the basal plane of stress-annealed pyrolytic graphite.

EXPERIMENTAL

The stress-annealed pvrolvtic graphite used in this study[a] has a X-ray rocking curve whose mosaic spread width is 0.3 to 0.4° at half-maximum intensitv of the (002) diffraction line. The measured 2d interplanar spacing is 6.713 ± 0.002 Å, as compared to 6.7078 ± 0.0002 Å for the single crystal (2).

The graphite electrodes with the basal plane exposed were

---

[a] Supplied by the Union Carbide Technical Center Research, Parma, Ohio 44130.

machined under compression into circular disks with a diameter of 5 mm. These graphite disks, backed with nickel to increase their mechanical strenght, were then press-fitted into a Teflon holder. The nickel backing was attached to the rear of the graphite electrode by means of silver epoxy cement (Eccobond Solder 58C, Emmerson-Cuming, Inc., Canton, Mass.) with electrical contact made to the nickel backing by a copper spring. An effort was made to establish whether the back junction between the nickel and the graphite contributed to the observed impedance. The electrode assembly was submerged in mercury and the impedance measured and found to be completely negligible.

A fresh electrode surface with the basal plane exposed was prepared for each experiment by placing a piece of plastic adhesive tape, cut to the exact size, in contact with the graphite surface and then peeling off a layer of graphite with the tape. Care was taken not to contaminate the Teflon surrounding the graphite disk with the adhesive on the plastic tape. The graphite surface so exposed had the appearance of a black mirror. Microscopic examination at 800X magnification revealed no plane other than the basal plane on the material with the $\sim 0.4^{\circ}$ rocking angle.

Electrodes made from a $\sim 8^{o}$ rocking angle sample were mechanically polished using different grade of alumina down to AB gamma (0.05 μ, Buehler Ltd.)

The electrochemical system included a counter electrode for the a.c. impedance measurements, an auxiliary electrode for d.c. polarizing the working electrode, and a reference electrode for measuring the d.c. potential of the working electrode. The main compartment of the all Teflon cell (Fig. 1) contained the working electrode and a 99.99% gold disk shaped counter electrode (9 cm diameter, 0.01 cm thick) located parallel to the working electrode at a distance of about 4 cm with one side pressed against the bottom of the Teflon cell. This electrode was used only for the a.c. impedance measurements in electrolytes at neutral pH. Gold was chosen for the counter electrode since it should not dissolve in helium-saturated neutral electrolytes. Test a.c. impedance measurements in 0.9 N NaF using a hydrogen-palladium (H/β-Pd) auxiliary electrode in a separate compartment without any gold electrode gave the same results as those with the gold counter electrode. For runs in acid solutions the gold counter electrode was removed and the a.c. measurements made versus the H/β-Pd

auxiliary electrode in the separate compartment. In the concentrated electrolytes the ohmic loss within the solution path leading to the separate compartment could be tolerated. In dilute solution, however, the use of a counter electrode within the main cell compartment was indispensable to minimize the ohmic loss in the electrolyte. Only neutral solutions were studied at low concentrations.

Two separate compartments connected to the central compartment contained the auxiliary and reference electrodes. Both of these electrodes were 99.99% palladium foil (2.9 cm diameter, 0.01 cm thick) over the rear of which was passed hydrogen gas (purified with an Engelhard Industries Pd-Ag alloy diffuser) in order to form a stable H/Pd alloy, the β phase (3). The reference compartment was connected to the main part via a Luggin capillary, while the auxiliary compartment was connected to the main compartment by a short tube (1 cm diameter, 5 cm long), filled with the same solution as the main compartment. The cell had a volume of 600 cm^3.

The experiments were performed in a nitrogen atmosphere glove box to reduce contamination by atmospheric components and to minimize possible incorporation of dust and dirt in the cell. Nitrogen gas obtained from boiling commercial liquid nitrogen (Linde) was continuously purged through the box. The temperature was maintained within the glove box at 25 $\pm$ 2^{o}C.

The solutions of sodium fluoride (Baker Analyzed Reagent) and sodium iodide (Fisher Scientific Co.) were prepared in nitrogen-saturated triple distilled water (second distillation from alkaline permanganate). The sodium sulfate solutions were prepared from a Baker reagent grade Na_2SO_4, recrystallized three times in triple distilled water. A 50% (by weight) solution of sodium hydroxide was prepared by dissolving Baker reagent grade pellets in triple distilled water in a Teflon bottle and then storing the saturated solution for several months to allow precipitation of sodium carbonate which has a very low solubility in such solutions ($\sim 10^{-4}$ M). The solutions used in experiments were then prepared by dilution and the concentration determined by titration with a standardized acid solution. The sulfuric acid solutions were prepared by diluting a distilled azeotropic solution (36.53 N). The azeotrope was prepared by distillation of du Pont reagent grade H_2SO_4 under reduce pressure with air slowly bleeding through the apparatus.

Trace contaminants were removed by treatment of the electrolytes (with the exception of the NaOH solutions) with active charcoal purified by extraction with hydrochloric acid for several months followed by washing with triple distilled water for months to remove the HCl. The active charcoal was then removed from the electrolytes using sintered glass. In acid and neutral solutions, *in situ* pre-electrolysis was performed with a 50 cm^2 gold cathode in the main compartment, polarized to -0.9 V vs H/β-Pd reference for at least

24 hr with agitation provided by bubbling purified helium through the solution. The alkaline solutions were pre-electrolysed in the same way with a 50-cm^2 nickel cathode. The pre-electrolysis electrodes were removed from the solution immediately after completion of the pre-electrolysis.

The helium gas used to de-aerate and to stir the solution was purified by passing it through a gas train, which included copper turnings maintained at about 450°C to remove O_2 and Linde type 3A and 13X molecular sieves, the latter in a liquid nitrogen trap, to remove other impurities.

In concentrated electrolytes (1 N), the measurements of the equivalent series capacitances and resistances were carried out at 25°C with an a.c. Wheatstone bridge and d.c. polarization circuit. The bridge has been checked with standard resistance and capacitance components and found to contribute a negligible error (< 1%) over the range of frequencies studied with this instrument (100 Hz to 20 kHz). The a.c. voltage applied to the cell did not exceed a few millivolts.

In dilute solutions ($\leq 10^{-2}$ N), difficulty was encountered with the bridge using sine waves because the high series resistance of the electrolyte (even with the counter electrode located close to the working electrode) resulted in inadequate sensitivity

to the interface impedance components, particularly the capacitive component. The use of lower frequencies is attractive to increase sensitivity to this interface capacitance but difficulty was encountered at lower frequencies (< 100 Hz) because of noise problems.

This situation has prompted the trying of a square wave bridge technique for the capacity measurements in dilute solutions. The a.c. oscillator of the bridge was replaced with a Hewlett-Packard function generator (model 3300A) as a source of square waves. This arrangment provides a sensitive method for independently balancing the series resistance and capacitance components without complications provided there is relatively small or no frequency dispersion. The situation is illustrated in Fig. 2 for various conditions of balance with an ideal series resistance - capacitance circuit and with an non-ideal series circuit in which the capacity is frequency dependent but the resistance near ideal. In this figure, oscillogram trace 3B corresponds to the balance of the capacity at the fundamental corresponding to the lowest frequency component of the Fourier series which can be used to represent the square wave. Unfortunately the facilities were not available to process the whole unbalanced signal and perform a Fourier transform so as to generate from a single measurement the complete frequency dependence curves for the capacitance and resistance components. The important point to note is that the sensitivity is still ample

to achieve a fairly precise capacitance balance for this low frequency component even in the presence of a high series resistance. With this square wave technique the gold counter electrode was used for both the impedance measurements and the polarization of the working electrode. Measurements carried out in 1 N, 0.1 N and 0.01 N electrolytes with both sine and square wave techniques gave identical results within the experimental error (i.e., a few %), provided the frequency at which the capacitance was measured with the square wave was taken to be the fundamental (see Fig. 4).

Delahay, de Levie, and Giuliani (4) have used a differential coulostatic charging method for differential capacitance measurements on mercury at concentrations down to 10^{-5} N. An attempt was made to use this method with the pyrolytic graphite electrodes but was not successful, principally because of small spurious faradaic processes which interfere more on graphite than on mercury.

All capacitances are given in terms of apparent electrode area. The true area has not been taken into account but the ratio of the true to apparent area should be essentially unity for the basal plane of stress-annealed pyrolytic graphite.

Current-voltage curves have been obtained by slow linear sweep voltammetry with a Wenking potentiostat and a solid state triangular wave generator[b]. An X-Y recorder (Mosley, model 7030A) was used to

---

[b] Designed by B.Cahan at Case Western Reserve University.

record the current as a function of potential.

RESULTS AND DISCUSSION

1. Basal plane of stress-annealed pyrolytic graphite ($\Delta\theta_{\frac{1}{2}} \simeq 0.4^{\circ}$)

In the earlier note (1), it has been shown that the frequency dispersion occuring in concentrated solutions at a disk electrode could be minimized by using a Teflon hood which provides a more uniform current distribution on the electrode. The same type of hood has been used in the present study; the internal diameter as well as the depth of the hood were 4 mm. The frequency dispersion of the capacity in concentrated NaF solutions is very small if the Teflon hood is slipped on to the electrode (see Fig. 4). In the absence of the hood, a frequency dispersion of the capacity is evident.

Beside providing a more uniform current distribution on the electrode, the hood restricted the effective area of the electrode to the center of the disk and hence minimized problems associated with other orientations which might be exposed along the periphery of the disk electrode where it comes in contact with the Teflon holder. This problem was of particular importance in the study of the basal plane of highly oriented pyrolytic graphite. The capacitance measured on the edge orientation was found to be at least one order of magnitude higher than on the basal plane, and hence even a small fraction of the surface other than the basal

orientation can lead to serious error. The need for the hood to eliminate complications with other orientations exposed at the periphery of the disk was further confirm with linear sweep voltammetry (Fig. 3). With the hood, the linear sweep voltammetry curves on the basal plane had no peaks in the range +1.0 to - 0.2 V vs NHE. Without the hood, peaks were evident and the curves less reproducible.

The electrode surfaces which were peeled off under the electrolyte with the hood then slipped on the wet surface exhibited greater frequency dispersion than those peeled off in air or in the N_2 - filled glove box with the hood then slipped on a dry surface (see Fig. 4). This frequency dispersion was attributed to the electrolyte film between the graphite surface and the Teflon hood. When the two surfaces are initially dry, the small gap between the hood and the portion of the graphite covered by it does not normally fill with electrolyte because of the hydrophobic nature of the two surfaces.

In neutral NaF solutions, however, it was found that the value of the capacity was more reproducible if the pyrolytic graphite was peeled off under the electrolyte rather than in air or in the N_2 - filled glove box. This dependence of the reproducibility on the way the pyrolytic graphite electrode has been renewed (peeled off wet or dry) is believed to be due to differences in the

quality or degree of perfection of the surfaces. In electrolytes other than NaF, the reproducibility of the capacitance was no longer dependent on the way the electrode has been prepared (peeled wet or dry). Futhermore, the shape of the capacity-potential curves was not dependent on whether the electrode surface was peeled off wet or dry.

The potential at which the measurements were made for Figs. 4 and 5 ($\sim$ + 0.2V vs NHE) corresponds normally to the open-circuit potential obtained immediately after dipping the electrode into the electrolyte. The frequency dispersion of the capacity does not depend on the electrode potential over the range of measurements (+0.5 to -0.5 V vs NHE) and is small for both the sine and square wave bridge techniques, both with and without the hood, in concentrated NaF solutions (> 0.1N).

The frequency dependence of the capacity on the basal plane of stress-annealed pyrolytic graphite measured with the sine and square wave techniques is shown in Fig. 5 for various concentrations of NaF (10^{-5} to 0.9 N). While both techniques give small frequency dispersion for the capacity in the more concentrated solutions, the apparent frequency dispersion (based on the fundamental) at 10^{-2}N and less is considerably less for the square wave than the sine wave technique. Below 10^{-4} N NaF the frequency dispersion even with the square wave technique is sufficiently pronounced that it

is necessary to go to lower frequencies than accessible in the present work to have a flattening of the capacity versus frequency curve. The lower frequency limit for the square wave measurements (7 Hz) was set by the lack of sufficient sensitivity below this value (signal-to-noise limited).

Most of the frequency dispersion residual even with the hood in the dilute solutions is believed to still result from non-uniform a.c. current distribution at the electrode. A higher length to diameter ratio for the hood would probably have been desirable for studies in the more dilute electrolytes but would have restricted the measurements because of excessive IR drop. This dispersion effect becomes less as the frequency is decreased since the interface capacity rather than the solution phase ohmic potential drop tends to become controlling. Consequently the capacity data at the lowest frequencies are believed to be prefered values for purposes of comparison at various electrolyte concentrations and potentials. This statement is in accord with the mathematical treatment recently given by Newman (5).

The capacity measured at a fixed potential on the basal plane decreased slowly with time. Most of the decrease occurred within the first 15 min and was usually smaller than 3% with electrodes peeled off wet while the series resistance remained virtually constant. This rate of decrease did not vary significantly with the applied potential in the range +0.5 to -0.5 V vs NHE or with stirring. The

rate of decrease was smaller with electrodes peeled off under electrolyte than peeled off dry.

The time dependence of the capacity on the basal plane was usually sufficiently small that the capacity-potential curves measured point by point were essentially the same regardless of whether the values were measured with increasingly anodic or cathodic potentials. If not specifically indicated, the values reported in the present study were recorded point by point with potential increasing in the anodic direction. The shape of the capacity-potential curves does not depend significantly on the way the electrode surface has been renewed (layer peeled off dry or wet).

The capacity-potential curves for the basal plane of stress-annealed pyrolytic graphite in NaF at concentrations from 0.9 N down to 10^{-5} N are represented in Fig. 6. Each curve is the average of at least 10 runs with the deviation between runs of about 5%. The shape of the capacity-potential curve is nearly symmetrical with respect to the minimum and does not exhibit the hump usually observed on metallic electrodes. The capacity at the minimum of the capacity-potential curve is low, i.e., about 3 $\mu f/cm^2$ in concentrated electrolyte, compared with values usually higher than 15 $\mu f/cm^2$ for metallic electrodes.

The series resistance in the impedance measurements in the very

dilute electrolytes was very high (e.g.> 2 X 10^6 ohms in 10^{-5} N NaF) with most of the resistance within the electrolyte bound by the hood. Even a very small steady residual d.c. current would have seriously interfered with the potentiostating of the working electrode to a fixed potential under such conditions. The fact that the potential of the minimum in the curves in Fig. 6 did not shift with concentration provides strong evidence that the residual current densities in the dilute electrolytes were very small (< 10^{-8} a/cm^2).

The ± 5% precision mentioned earlier makes it difficult to establish the small electrolyte concentration dependence of the shape of the capacity-potential curves and by how much they are translated downward with decreasing concentration. The most significant point is that the minimum capacitance at low concentration is still far higher than is to be expected on the basis of the series equivalent diffuse ionic layer capacity at the ordinary point of zero charge. For example, according to the Gouy-Chapman theory (see, for example ref. 6), for a 10^{-5} N NaF solution, the diffuse ionic layer capacity should be C_d = 0.72 $\mu f/cm^2$ at the rational potential zero, whereas the minimum in Fig. 6 is about 1.7 $\mu f/cm^2$. Furthermore, the capacity-potential curves at low concentrations in Fig. 6 do not show the deep minimum to be expected if the experimental minimum corresponds to the effective potential of zero charge (pzc) for the ionic double layer. This means that either the pzc for the ionic double layer is outside the potential range studied or the electrode

surface is more heterogeneous than expected, perhaps due to imperfections where the edge orientation is exposed. Each of these possibilities will be considered.

The minimum in the capacity-potential curves in Fig. 6 is present even at high electrolyte concentrations and is attributed to the space charge region within the graphite as will be discussed later. To a first approximation, the effect of going to lower concentration in Fig. 6 may be viewed as a simple downward translation of the curves with only a slight sharpening up of the minimum. If the space charge and compact double layer capacities are assumed constant with concentration, a series diffuse ionic layer capacitance contribution of approximately 7.6 and 3.9 $\mu f/cm^2$ would be required to account for the downward displacement of the 10^{-4} and 10^{-5} N curves, respectively, relative to the 0.9 N NaF curves, assuming also that the diffuse layer capacitances are independent of electrode potential over the voltage range studied. This assumption is reasonable if most of the applied potential change occurs across the space charge region within the graphite and hence results in only a quite small change in the potential across the diffuse ionic layer (ϕ_2). According to the Gouy-Chapman theory, the diffuse ionic layer capacity is proportional to the square root of the ionic concentration and hence the ratio of the diffuse ionic layer capacity at 10^{-4} N to that at 10^{-5} N should be $\sim$ 3 to 1, as compared with the $\sim$ 2 to 1 ratio represented by the values of 7.6 and 3.9 $\mu f/cm^2$ mentioned earlier. This difference

is probably not experimentally significant in view of the experimental scatter of the capacity data with freshly prepared surfaces mentioned earlier. These values, however, are much higher than computed for the diffuse ionic layer capacity at ϕ_2. For the 10^{-5} N solution, the diffuse ionic layer capacity of 3.9 $\mu f/cm^2$ corresponds to ϕ_2 = .12 V according to the Gouy-Chapman theory (see e.g., ref. 6). Since the effect of changing ionic concentration is principally to translate the capacity-potential curves along the capacity ordinate, this implies that the pzc for the diffuse ionic layer is outside the potential range studied.

In the absence of surface states, the potential of the minimum in the capacity of the diffuse part of the ionic double layer may be expected to coincide with the flat band potential, i.e., the point zero of space charge (7). Fig. 7 gives a schematic representation of the potential distribution at a semiconductor-electrolyte interface with and without the contribution of surface states of a chemical origin. With surface states present at the semiconductor surface, the potential drop in the diffuse ionic layer may no longer be close to that in the space charge layer within the semiconductor and consequently the flat band potential (i.e., for $\Delta\phi_{sc} = 0$) would not coincide with the minimum in the Helmoltz layers. Our possible source of such surface states is chemical interactions between the graphite and solution phase species, perhaps at imperfections on the electrode surface exposing edge orientations.

The possibility cannot be ruled out that the effective pzc for the ionic double layer does fall at the effective flat band potential and at the minimum of the curves in Fig. 6, but does not show up as

the sharp minimum normally found on such surfaces as mercury because of some type of surface heterogeneity. The minimum in the capacity-potential curves does become slightly sharper at lower concentrations in Fig. 6. If the surface heterogeneity is caused by surface imperfections, the concentration of such might be sufficiently low for them to be separated by distances large compared to the effective thickness of either the ionic diffuse layer even at electrolyte concentrations of 10^{-5} to 10^{-4} N (corresponding to charge carrier concentrations of 10^{16} to 10^{17} per cm^3) or the space charge region within the graphite with its carrier concentration of $\sim 10^{19}$ per cm^3. Under such circumstances (with a bit of contriving), the minima in the space charge capacity as well as the diffuse ionic layer capacity might be much broader than normal. If such imperfections involve exposed edge orientations, they would be expected to have ionizable groups attached (acidic or basic) and to be pH dependent. As will be reported later in this paper, no appreciable pH dependence of the minimum in the capacity-potential curve has been observed, however.

On metal electrodes the F^- ion is known to exhibit very little tendency for specific adsorption whereas halide ions such as the iodide ion normally specifically adsorb quite strongly. This behavior was checked on the basal plane of stress-annealed pyrolytic graphite by running the same measurements in NaI as those previously described in NaF. In the NaI solutions, the results were found to be more sensitive to the surface preparation of the electrode than with NaF solutions. Nevertheless, measurements carried out in 0.8 N NaF + 0.1 N NaI and in 0.9 N NaF + 0.01 N NaI did not show any measurable difference from those obtained in 0.9 N NaF (see Fig. 8).

This result is quite different from those reported for metallic electrodes where the specific adsorption of the iodide leads to a substantial increase in the capacity relative to that with only fluoride anions present, especially on the anodic potential side (8).

Capacity-potential measurements also have been performed in other 1 N electrolytes in order to study the influence of the pH on the potential of the minimum capacity. In all 1 N electrolytes studied, the frequency dependence of the capacity was approximately the same as that reported in 0.9 N NaF (Fig. 4). Capacity-potential curves obtained in 1 N H_2SO_4 and in 1 N NaOH are reported in Fig. 9. These curves are very similar to that reported in NaF electrolyte. For runs at pH = 3 and = 11, Na_2SO_4 was used as the principal electrolyte with addition of H_2SO_4 or NaOH to adjust the pH to the desired value. Runs at pH = 6 and = 8 were carried out in NaF with addition of HF. Neither the potential of the minimum capacity (Fig. 10) nor the capacity at the minimum (Fig. 11) were found to be dependent on the pH or anion on the basal plane of stress-annealed pyrolytic graphite within the experimental precision. The scatter of capacitance data measured at various pH, however, is substantial as can be seen on Fig. 11. This lack of reproducibility of the capacitance data measured on the basal plane of stress-annealed pyrolytic graphite may arise from the following:

1) Surface imperfections and possibly the presence of traces of amorphous carbon may contribute significantly to the capacitance component according to their nature and relative number. These may vary substantially as each new surface is prepared by peeling.

2) Despite the purification procedure, the impurities in the electrolyte may adsorb on the graphite surface and give rise to different surface states, affecting the capacity.

3) The experimental geometry, limited by the Teflon hood, may fluctuate slightly from one experiment to the other depending on the pressure applied in slipping the hood on to the graphite electrode.

Of these, the authors believe that the first is most important.

An effort has been made to establish if there are any faradaic processes such as hydrogen discharge or any non-faradaic adsorption-desorption processes in the potential range involved in the a.c. impedance measurements. Slow linear sweep voltammetry on the basal plane of the stress-annealed pyrolytic graphite in 0.9 N NaF (pH ≈ 6), 1 N H_2SO_4, and 1 N NaOH (see Figs. 3 and 9) reveals a peak in the cathodic sweeps at potentials in the range ∿ -0.3 to -0.6 V vs NHE with the areas under the cathodic peak corresponding to 10 - 30 $\mu coul/cm^2$, depending on the electrolyte. This peak may be caused by either ion adsorption-desorption or the reduction of a species which adsorbed on or is part of the surface or diffusing to it from within the solution phase. Further studies of this voltammetry peak, particularly as a function of voltage scan rate, are necessary before the processes responsible for it can be identified. The reduction of adsorbed species or functional groups present on misoriented portions of the surface arising from surface imperfections does not seem a highly probable explanation since too large a fraction of the surface area would need to be involved (up to ∿ 10%) to account for the number of coulombs associated with the peak.

Hydrogen evolution occurs at appreciable rates ($> 10^{-3} a/cm^2$) only at hydrogen overpotentials of $\sim$ 1.0V or greater on the basal plane.

The peak in the voltammetry curves in Figs. 3 and 9 does occur at potentials in the range of the a.c. impedance measurements, and yet, no abnormality in the capacity-potential curves is observed at these potentials. The apparent differential capacity calculated for the peak from the maximum peak current density and the potential sweep rate is of the order of $100 \mu f/cm^2$ in the NaF and H_2SO_4 solutions, which is two orders of mangitude higher than the differential capacitance values obtained from the a.c. impedance measurements. Furthermore, even in the regions of the voltammetry curves where the currents are relatively constant, the apparent differential capacities estimated from the differences in anodic and cathodic sweep current densities and the potential sweep rates are still $\sim 20 \mu f/cm^2$ in the NaF, H_2SO_4, and NaOH solutions (with hood), or approximately one order of magnitude higher than the values from the a.c. impedance measurements. This difference in differential capacitance estimated from the voltammetry curves and the a.c. impedance measurements is not unusual with metal electrodes and in the present case may occur because of a portion of the surface has a microorientation which exposes other than the basal plane or because of the presence of even amorphous carbon (or soot) over a small part of the surface.

2. Basal plane with rocking angles greater than 0.4°

Samples of pyrolytic graphite with decreasing crystal perfection were studied in 0.9 N NaF and their behavior compared to that observed on the samples with the lowest rocking angle available ($\Delta\theta_{1/2}$ = 0.3 to 0.4°). No significant differences in the shape of the capacity-potential curves or in the minimum value of the capacity were observed on the basal plane of samples with rocking angles of 0.4, 0.8, 1.2 and ∿ 4°. With ∿ 8° rocking angle some deviations are evident (see Fig. 12). The curve reported in Fig. 12 is essentially the same for points measured with increasing or decreasing anodic potential. The irregularities observed are attributed to the influence of some microorientations other than the basal plane.

The sample with ∿ 8° rocking angle is an interesting one because its basal plane surface can be renewed both by peeling off a layer and by polishing. Samples with lower rocking angle cannot be polished without producing a surface of very poor homogeneity to the eye and those with higher rocking angles cannot be peeled off. The comparison between the behavior of the polished and the peeled-off surfaces of the same sample (Fig. 13) shows that:

1. The polished sample has a minimum capacity about 5 times higher than the peeled one.
2. On the peeled off surface the anodic and cathodic sweep of the capacity-potential curves show negligibly small hysteresis whereas on the polished surface the shape of the cathodic sweep curve (potential going negative) depends on the maximum positive potential applied.

In contrast, the anodic sweep is reproducible. As it will be seen in a further publication, this behavior is observed on the edge orientation of pyrolytic graphite as well as on the glassy carbon.

These differences in behavior between polished and peeled samples probably are the result of the much greater amount of edge orientation on the basal plane exposed by the polishing procedure.

The different behavior between cleaved and polished pyrolytic graphite electrodes has been studied by Bauer et al.(9). These authors reported values of capacities ranging from $\sim$ 12μf/cm^2 for the surface prepared by cleaving to $\sim$ 60μf/cm^2 for the polished basal plane of ordinary pyrolytic graphite measured at 1000 Hz. (also a 1:5 ratio).

Ordinary pyrolytic graphite (as-deposited material) has been used in various electrochemical studies by different authors and its behavior was also of interest. Fig. 14 shows the results obtained with such a polished sample whose rocking angle was about 40°. The capacity-potential curve is not very different from that measured on the polished basal plane with a rocking angle of $\sim$ 8° (Fig. 13) although the minimum value (18μf/cm^2) is slightly higher and the hysteresis between the anodic and cathodic sweep more pronounced for the ordinary pyrolytic graphite than for the sample with the $\sim$ 8° rocking angle. The insert in Fig. 14 gives the capacity-potential curve based on data reported by Bauer et al. (9) for the ordinary pyrolytic graphite in 0.5 N KCl at 1000 Hz. The surface of their sample was renewed by polishing, as it was the case in the measurements reported in the present study. The shape of the capacity-potential curve measured with increasingly cathodic potentials reported

by Bauer et al. for the ordinary pyrolytic graphite is somewhat similar to that obtained in the present study for a similar material in the same cathodic direction. However, the hysteresis between the two anodic and cathodic sweeps was not noted by these authors in their publication and the absolute value of the capacity reported by Bauer et al. is twice as high as that found in the present study.

Atanasoski et al. (10) have measured the differential capacity of ordinary pyrolytic graphite in aqueous sodium sulfate solution. Samples were polished, subjected to an argon atmosphere at 1000°C and dipped into electrolyte without contact with the external atmosphere. The absolute value of the capacity at the minimum of the capacity-potential curves are about two fold higher than those reported in the present study (Fig. 14). The capacity-potential curves are similar with the potentials of the minimum close in value. Atanasoski et al., however, found less hysteresis from anodic to cathodic measurements. The diffirent origin and particularly preparation of the samples are probably responsible for these differences. Atanasoski et al. found the capacity-potential curves to be of the same shape for electrolyte concentrations from 0.014 to 0.8 N, as was also found for the highly oriented pyrolytic graphite (basal plane) in the present work.

The variation of the frequency dependence of the capacity as a function of the rocking angle of the samples is illustrated in Fig. 15. The frequency dispersion is more pronounced for the peeled sample with a rocking angle of $\sim 8^\circ$ than that noted previously on the stress-annealed material with $\sim 0.4^\circ$ rocking angle. For the most part, the hood takes care of frequency dispersion arising from non-uniform current distribution, in the relatively

concentrated electrolytes. Therefore the significant frequency dispersion observed at higher rocking angles is attributed to surface roughness and/or relaxation phenomena involving surface states. The authors believe the former to be the most likely source of this frequency dispersion. The difference in the frequency dispersion between the sample peeled off dry or wet is essentially the same as that reported for the most highly oriented material. If the basal plane of pyrolytic graphite is polished, rather than prepared by the peeling technique, however, the frequency dependence of the capacity increases very susbstantially. The frequency dispersion of the capacity reported in the present study appears reasonable compared to that described in the literature for polycrystals (11) or porous electrodes (12).

Linear sweep voltammetry performed on the basal plane of stress-annealed pyrolytic graphite with $\sim 8^\circ$ rocking angle (Fig. 13) reveals two different curves according to the way the surface has been renewed. The peeled sample (curve B, Fig. 13) has almost the same behavior as that of the sample with $\sim 0.4^\circ$ rocking angle (Fig. 3, curve A). When the electrode surface has been renewed by polishing (curve A, Fig. 13), the shape of the current-potential curve is a combination of those measured on the basal and edge planes of the highly oriented material (Fig. 3, curves A and C). On the polished basal plane of ordinary pyrolytic graphite (Fig. 14), the linear sweep voltammetry reveals a broad peak in the anodic sweep at about +0.4 V vs NHE whose peak height is less than that observed on the edge orientation (Fig. 3, curve C). Polishing of the basal plane produces a surface which exposes edge orientations on a microlevel. The presence of various chemical groups and

adsorbed species on the edge orientation results in peaks in the voltammetry curves, more complex capacity potential curves and rather pronounced hysteresis effects.

3. Other graphite and carbon electrodes

The capacity-potential curves for boronated stress-annealed pyrolytic graphite and glassy carbon as well as the edge orientation of stress-annealed pyrolytic graphite were also studied. The shape of the capacity-potential curve of the boronated material is more complicated than with the undopped material. The potential of the minimum capacity is shifted towards more negative values by about 0.5 V where the capacity value is $\sim$ 4.5 $\mu f/cm^2$. On the edge orientation of stress-annealed pyrolytic graphite and on glassy carbon the capacity-potential curve is reproducible only in the anodic direction (potential going positive) whereas the shape of the cathodic branch depends on the maximum positive potential applied. The minimum value of the capacity is $\sim$ 50 $\mu f/cm^2$ for the edge orientation and $\sim$ 13 $\mu f/cm^2$ for the glassy carbon in 0.9 N NaF. The potential of the minimum of the capacity-potential curve is pH dependent, contrary to the behavior on the basal plane. These results will be presented in a further publication.

SIGNIFICANCE OF RESULTS

The low value of the apparent capacity of the basal plane of stress-annealed pyrolytic graphite at the minimum of the capacity-potential curve has been explained earlier (1) using the semiconductor theory. The differential capacitance of a semiconductor or semi-metallic electrode-electrolyte interface is composed of three series components: the capacitance of the space charge layer within the semiconductor, that of the compact double layer, and that of the diffuse ionic layer of the electrolyte. For electrolytes of high concentrations, e.g., 1 M, the capacitance of the diffuse ionic layer is usually large, i.e., > 100μf/cm^2, compared to the other two components. In this case, its contribution to the total capacitance is therefore small The capacitance associated with the compact layer is expected to have a value of 15 to 20μf/cm^2 in the absence of surface states on the basis of the values encountered with metal electrodes. The capacity of the compact double layer on the basal plane of graphite may differ appreciably from the value for metals due to the unusual electronic nature of the graphite surface but it seems quite unlikely that this difference would amount to almost an order of magnitude. Consequently, the low observed capacity is best attributed to the space charge component within the graphite.

The theory of semiconductor electrodes indicates that the capacitance of the space charge layer in a pure intrinsic semiconductor should exhibit a minimum value given by the expression (13):

$$C_o = \left[\frac{2\,\varepsilon\varepsilon_o\, e^2\, c}{kT}\right]^{\frac{1}{2}} \qquad (2)$$

with the dependence of the capacity on potential given as:

$$C_{sc} = C_o \cosh\left(\frac{\phi\, e}{2kT}\right) \qquad (3)$$

where ε = dielectric constant

ε_o = permittivity

e = absolute value of electronic charge

c = electronic charge carrier density

k = Boltzmann's constant

T = absolute temperature

ϕ = potential at the surface

The electronic charge carrier density has been reported to be $6 \cdot 10^{18}$ (14), $5.5 \cdot 10^{18}$ (15) and $7 \cdot 10^{18}$ carriers/cm^3 (16) for heat-treated pyrolytic graphites similar to those used in the present study. The only values apparently available for the dielectric constant are those from optical measurements rather than at audio frequencies. According to Ergun et al. (17) the value of ε at 5461 Å in the basal plane is 2.61 and along the c-axis is 3.28. Using the value of $6 \cdot 10^{18}$ carriers/cm^3 for the electronic carrier concentration (mean value from ref. 14, 15 and 16) and 3 for the dielectric constant (17), C_o is 4.5μf/cm^2 as compared to about 3μf/cm^2 for the experimental value. The comparison of the calculated C_o value with the experimental

value is reasonable, considering the uncertainty as to c and ε.

The shift of the potential at the minimum capacity for the boronated sample with respect to the unboronated material also is in good agreement with the semiconductor interpretation since the boronated sample exhibits p-type semiconducting characteristics which should shift the flat band potential towards more negative potentials than that observed on the intrinsic stress-annealed pyrolytic graphite.

The potential dependence of the space charge capacity represented by eq. (3) is much greater than that observed experimentally on the basal plane of stress-annealed pyrolytic graphite (Fig. 6). Possible factors responsible for this discrepancy are:

a) imperfections on the exposed basal plane, giving rise to sites other than those with completely satisfied valencies and resulting in degenerate surface electronic states. In the case of germanium electrodes, Gerischer (18) has given a theoretical treatment which shows that the space charge capacity depends relatively little on polarization in the potential region of surface degeneracy.

b) The applicability of the presently available semiconductor theory to a system such as graphite with a total carrier concentration as high as 10^{19} carriers/cm^3 and hence with Debye lengths comparable to the lattice demension is open to serious question.

Neither the minimum capacity nor the potential at which it occurs in the basal plane of stressed-annealed pyrolytic graphite have any appreciable dependence on pH or the type of ions. This is in strong contrast to the behavior reported with semiconductor electrodes such as germanium (19-20) as well as with metal electrodes and suggests that such graphite surfaces are relatively free of functional groups such as OH, H and other surfaces species which strongly interact with ions of the electrolyte.

ACKNOWLEDGMENT

The authors are pleased to acknowledge the support of this research by the U.S. Office of Naval Research. One of us (J.-P.R.) thanks the Stiftung für Stipendien auf dem Gebiete der Chemie, Basel, Switzerland for the award of a Research Fellowship. The authors also express appreciation to the Union Carbide Technical Center, Parma, Ohio and Dr. A. Moore of that laboratory for providing the various pyrolytic graphites used in this study. The authors also express their appreciation to Dr. Boris Cahan for valuable discussion.

REFERENCES

1. J.-P. Randin and E. Yeager, J. Electrochem. Soc. 118,711 (1971).

2. W.N. Reynolds, "Physical Properties of Graphite", Elsevier Pub., Amsterdam, p. 2 (1968).

3. D.J.G. Ives and G.I. Janz, "Reference Electrodes", Academic Press, New York, p. 112-116 (1961).

4. P. Delahay, R. de Levie and A.M. Giuliani, Electrochem. Acta 11, 1141 (1966).

5. J. Newman, J. Electrochem. Soc. 117, 198 (1970).

6. P. Delahay, "Double Layer and Electrode Kinetics", Interscience Pub., New York, p. 33 (1965).

7. V.A. Myamlin and Y.V. Pleskov, "Electrochemistry of Semiconductor", Plenum Press, New York, p. 84 (1967).

8. E. Duthiewicz and R. Parsons, J. Electroanal. Chem. 11, 100 (1966).

9. H.H. Bauer, M.S. Spritzer and P.J. Elving, J. Electroanal. Chem. 17, 299 (1968).

10. R.T. Atanasoski, D.M. Drazhich and A.R. Despich, Elektrokhimiya 6, 1200 (1970).

11. ref. 6, p. 130.

12. R. de Levie, Electrochem. Acta 10, 113 (1965).

13. H. Gerischer, in "Advances in Electrochemistry and Electrochemical Engineering", Ed. by P. Delahay, Vol. 1, p. 155, Interscience Pub., New York, (1961).

14. C.A. Klein, J. Appl. Phys. 33, 3338 (1962).

15. C.A. Klein and W.D. Straub, Phys. Rev. 123, 1581 (1961).

16. C.A. Klein, Rev. Mod. Phys. 34, 72 (1962).

17. S. Ergun, J.B. Yasinsky and J.R. Townsend, Carbon 5, 403 (1967).

18. ref. 13, p. 160.

19. H. Gerischer, in "Physical Chemistry, An Advanced Treatise", Vol. IXA, Electrochemistry, Ed. by H. Eyring, Academic Press, New York, p. 487 (1970).

20. P.J. Boddy, J. Electroanal. Chem. 10, 199 (1965).

LIST OF FIGURES

Fig. 1 Electrochemical cell for a.c. impedance and linear sweep voltammetry measurements. (Reference electrode (RE), auxiliary electrode (AE) and hood not shown.)

a = Working electrode
b = Luggin capillary
c = Gold counter electrode
d = Teflon
e = Electrolyte level
f = Entrance for pre-electrolysis electrodes and gas outlet
g = Metal shaft
h = Helium inlet

Fig. 2 Bridge balancing with square waves
A) Ideal series capacitance and resistance circuit

1) C balanced; R unbalanced
2) C unbalanced; R balanced
3) C and R balanced

B) Series capacitance-resistance circuit with frequency dependent C and frequency independent R

1) C low frequency balanced; R unbalanced
2) C low frequency unbalanced; R balanced
3) C low frequency balanced, R balanced

Fig. 3 Current-potential curves for the basal plane of stress-annealed pyrolytic graphite ($\Delta\theta_{\frac{1}{2}} \cong 0.4^{\circ}$) with and without hood, as well as for the edge orientation of the same material in 0.9 N NaF at 25°C. Scan rate 0.1 V/sec., direction of sweep indicated by arrows.

A) on the basal plane of stress-annealed pyrolytic graphite, with hood, layer peeled off dry,
B) same as A, without hood,
C) on the edge orientation of the same material, resurfaced by polishing, without hood.

Fig. 4 Frequency dependence of capacitv for the basal plane of stress-annealed pyrolytic graphite ($\Delta\theta_{\frac{1}{2}} \approx 0.4^{o}$) in 0.9 N NaF at 25°C at a potential of ~ +0.2 V vs NHE

Sine wave : ▫ without hood, layer peeled off wet
o with hood, layer peeled off dry
Δ with hood, layer peeled off wet

Square wave : ■ without hood, layer peeled off wet
● with hood, layer peeled off dry
▲ with hood, layer peeled off wet

Fig. 5 Frequency dependence of capacity for the basal plane of stress-annealed pyrolytic graphite ($\Delta\theta_{\frac{1}{2}} \approx 0.4^{o}$) in NaF solutions at 25°C and at a potential of about +0.2 V vs NHE; with hood, layer peeled of dry

x 0.9 N, square wave
o 0.9 N, sine wave
Δ 0.1 N, square wave
▲ 0.1 N, sine wave
▫ 0.01 N, square wave
■ 0.01 N, sine wave
● 10^{-3} N, square wave
+ 10^{-4} N, square wave
● 10^{-5} N, square wave

Fig. 6 Capacity-potential curves for the basal plane of stress-annealed pyrolytic graphite ($\Delta\theta_{\frac{1}{2}} \approx 0.4^{o}$) in NaF solutions (pH ≈ 6) at 25°C and 20Hz, with hood, layer peeled off dry

x 0.9 N;
o 10^{-1} N;
+ 10^{-2} N;
● 10^{-3} N;
Δ 10^{-4} N;
▲ 10^{-5} N;

Fig. 7 Schematic representation of potential distribution at the basal plane of the pyrolytic graphite/electrolyte interface

A) without appreciable contribution from surface states:

1) general case
2) at the flat band potential = point of zero charge

B) with contribution from surface states:

1) general case
2) at the flat band potential, $\Delta\phi_{sc}$ = 0

Fig. 8 Capacity-potential curves for the basal plane of stress-annealed pyrolytic graphite ($\Delta\theta_{\frac{1}{2}} \cong 0.4^{o}$) in NaF + NaI solutions (pH ≈ 6) at 25°C and 1000 Hz (sine wave), with hood, layer peeled off dry

x 0.9 N NaF
o 0.8 N NaF + 0.1 N NaI
Δ 0.9 N NaF + 0.01 N NaI

Fig. 9 Capacity-potential and current-potential curves for the basal plane of stress-annealed pyrolytic graphite ($\Delta\theta_{\frac{1}{2}} \cong 0.4^{o}$) in 1 N H_2SO_4 and 1 N NaOH solutions at 25°C and 1000 Hz (sine wave), with hood, layer peeled off dry

x 1 N H_2SO_4 ; o 1 N NaOH

Scan rate for the current-potential curves 0.1 V/sec, direction of sweep indicated by arrows

A) 1 N H_2SO_4 ; B) 1 N NaOH

Fig. 10 pH dependence of the electrode potential for the minimum capacity for the basal plane of stress-annealed pyrolytic graphite ($\Delta\theta_{\frac{1}{2}} \cong 0.4^{o}$) at 25°C

Fig. 11 pH dependence of the minimum capacity for the basal plane of stress-annealed pyrolytic graphite ($\Delta\theta_{\frac{1}{2}} \cong 0.4^{o}$) at 25°C. (Each point corresponds to a new surface prepared by the peeling technique.)

Fig. 12 Capacity-potential curves for the basal plane of annealed pyrolytic graphite with $\Delta\theta_{\frac{1}{2}} \cong 8^{o}$, in 0.9 N NaF (pH ≈ 6) at 25°C and 1000 Hz (sine wave), with hood, layer peeled off under electrolyte

x experimental points for annealed pyrolytic graphite with $\Delta\theta_{\frac{1}{2}} \cong 8^{o}$

---- comparison curve for the stress-annealed pyrolytic graphite with $\Delta\theta_{\frac{1}{2}} \cong 0.4^{o}$

Fig. 13 Capacity-potential and current-potential curves for the basal plane of annealed pyrolytic graphite ($\Delta\theta_{\frac{1}{2}} \cong 8^{o}$) in 0.9 N NaF (pH ≈ 6) at 25°C and 1000 Hz (sine wave), with hood.
Scan rate for the current-potential curves 0.1 V/sec, direction of sweep indicated by arrows

A) surface renewed by polishing
. . ———— potentials scanning positive from -0.8 V vs NHE
— — — — — potentials scanning negative from 0.1 V vs NHE
—— — — potentials scanning negative from 0.4 V vs NHE
—·—·— - potentials scanning negative from 0.7 V vs NHE
— - - - - - potentials scanning negative from 1.0 V vs NHE

B) Surface renewed by peeling off a layer.

Fig. 14 Capacity-potential and current-potential curves for the basal plane of ordinary pyrolytic graphite ($\Delta\theta_{\frac{1}{2}} \approx 40^{o}$) in 0.9 N NaF (pH ≈ 6) at 25°C and 1000 Hz (sine wave), with hood, surface renewed by polishing
Scan rate for the current-potential curves 0.1 V/sec, direction of sweep indicated by arrows

——— potentials scanning positive from -0.5 V vs NHE
– – – – potentials scanning negative from 0.1 V vs NHE
— — — potentials scanning negative from 0.4 V vs NHE
—·—·— potentials scanning negative from 0.7 V vs NHE
· · · · · · · · potentials scanning negative from 0.9 V vs NHE

Insert figure: Bauer, Spritzer and Elving [9] data in 0.5 N KCl, resurfaced by polishing, frequency 1000 Hz.

Fig. 15 Frequency dependence of capacity for the basal plane of pyrolytic graphite with different crystalline perfections in 0.9 N NaF at 25°C, with the sine wave method, with hood

x ordinary pyrolytic graphite ($\Delta\theta_{\frac{1}{2}} \approx 40^{o}$), polished
o annealed pyrolytic graphite ($\Delta\theta_{\frac{1}{2}} \approx 8^{o}$), polished
Δ annealed pyrolytic graphite ($\Delta\theta_{\frac{1}{2}} \approx 8^{o}$), layer peeled off dry
----- stress-annealed pyrolytic graphite ($\Delta\theta_{\frac{1}{2}} \approx 0.4^{o}$), layer peeled off dry.

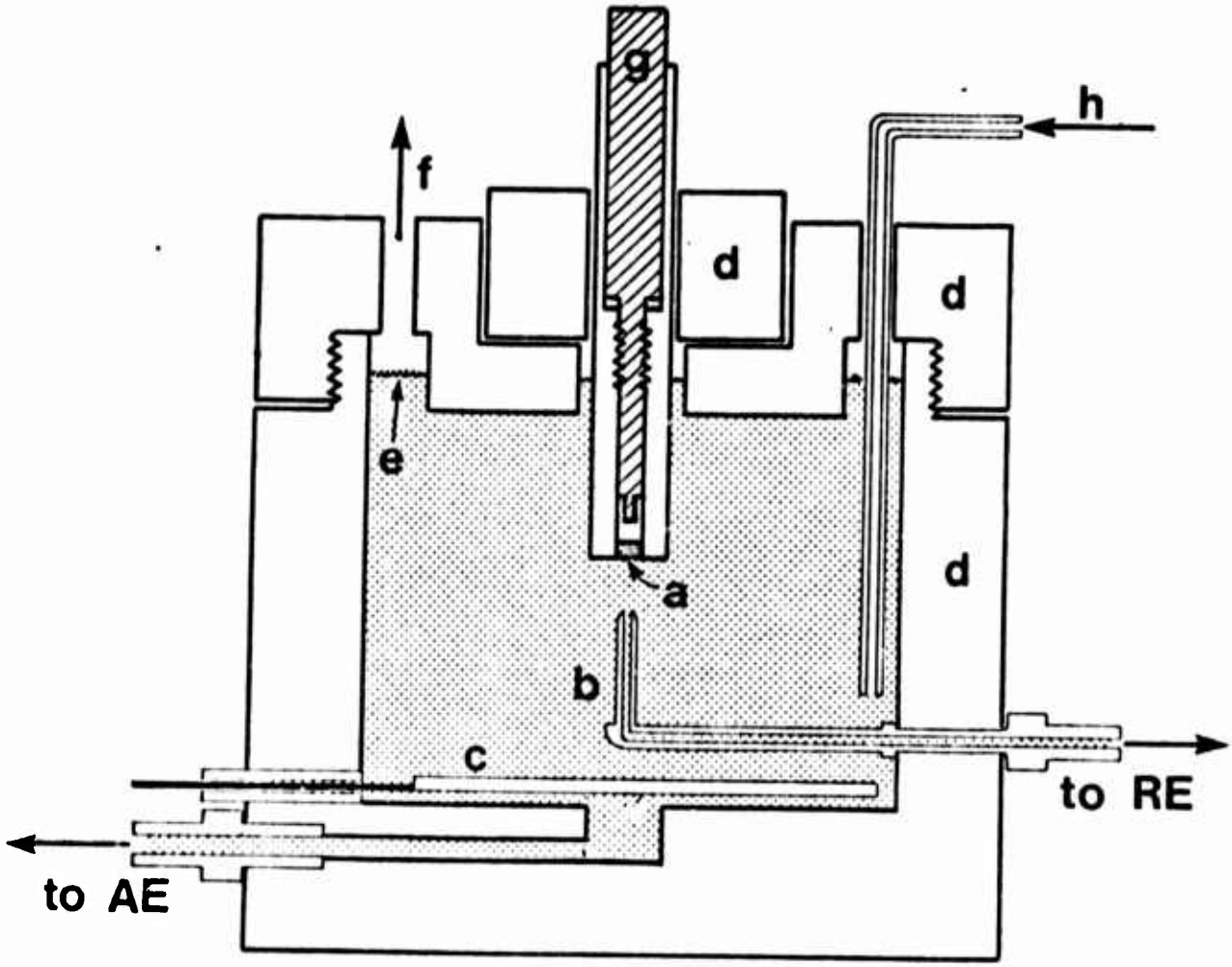

Fig. 1 Electrochemical cell for a.c. impedance and linear sweep voltammetry measurements. (Reference electrode (RE), auxiliary electrode (AE) and hood not shown.)

a = Working electrode
b = Luggin capillary
c = Gold counter electrode
d = Teflon
e = Electrolyte level
f = Entrance for pre-electrolysis electrodes and gas outlet
g = Metal shaft
h = Helium inlet

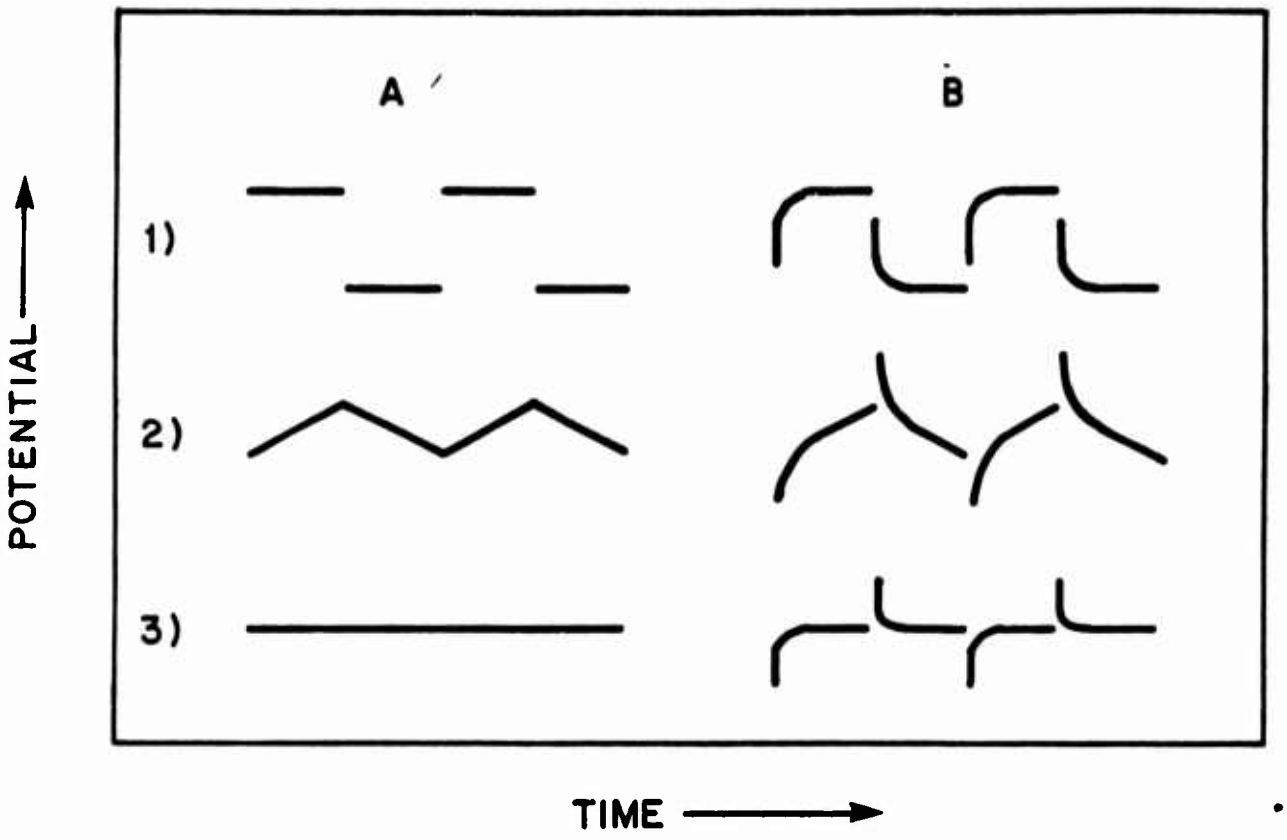

Fig. 2 Bridge balancing with square waves
A) Ideal series capacitance and resistance circuit

1) C balanced; R unbalanced
2) C unbalanced; R balanced
3) C and R balanced

B) Series capacitance-resistance circuit with frequency dependent C and frequency independent R

1) C low frequency balanced; R unbalanced
2) C low frequency unbalanced; R balanced
3) C low frequency balanced, R balanced

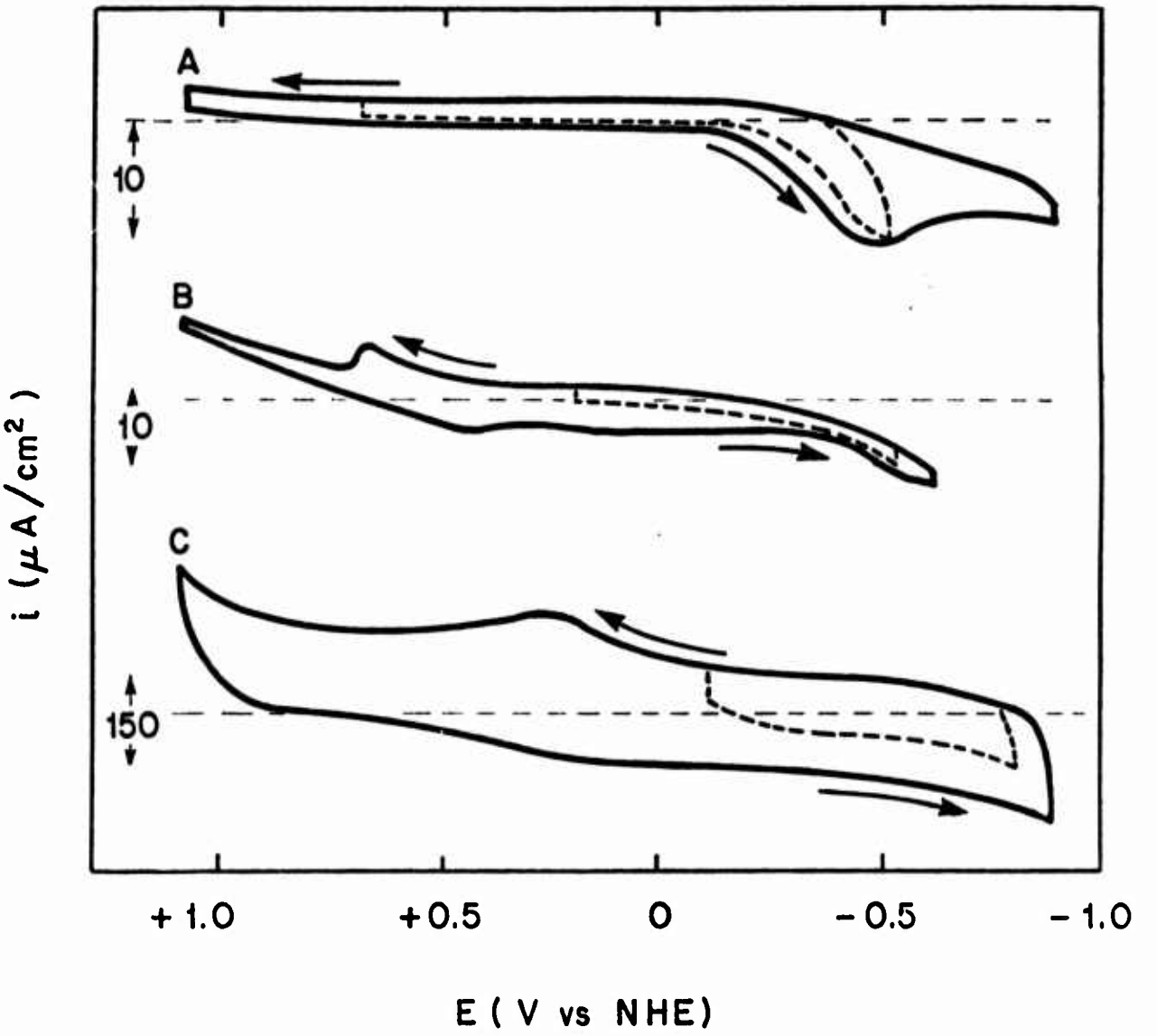

Fig. 3 Current-potential curves for the basal plane of stress-annealed pyrolytic graphite ($\Delta\theta_{\frac{1}{2}} \cong 0.4°$) with and without hood, as well as for the edge orientation of the same material in 0.9 N NaF at 25°C. Scan rate 0.1 V/sec., direction of sweep indicated by arrows.

A) on the basal plane of stress-annealed pyrolytic graphite, with hood, layer peeled off dry,
B) same as A, without hood,
C) on the edge orientation of the same material, resurfaced by polishing, without hood.

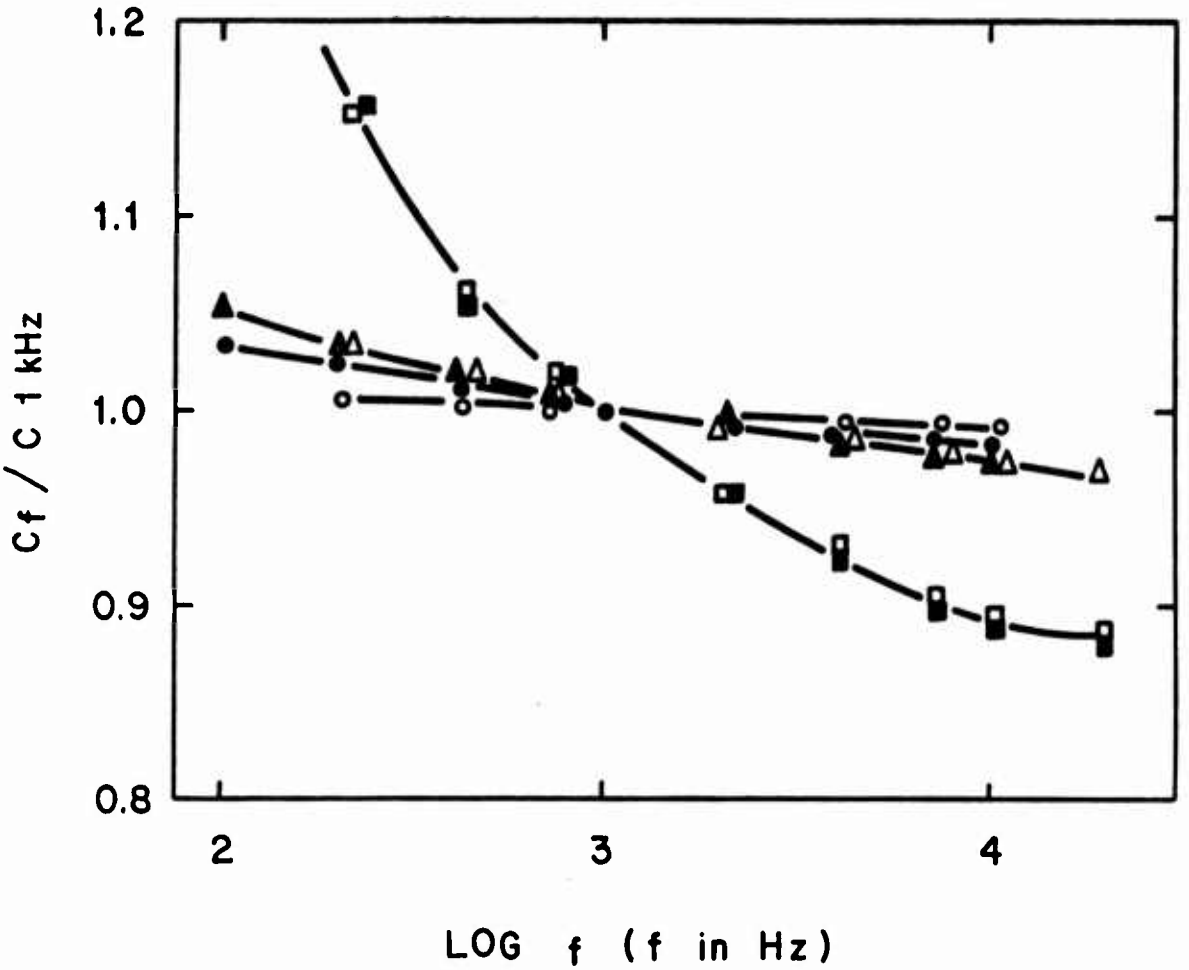

Fig. 4 Frequency dependence of capacity for the basal plane of stress-annealed pyrolytic graphite ($\Delta\theta_1 \cong 0.4°$) in 0.9 N NaF at 25°C at a potential of ∿ +0.2 V vs NHE

Sine wave : □ without hood, layer peeled off wet
o with hood, layer peeled off dry
Δ with hood, layer peeled off wet

Square wave: ■ without hood, layer peeled off wet
● with hood, layer peeled off dry
▲ with hood, layer peeled off wet

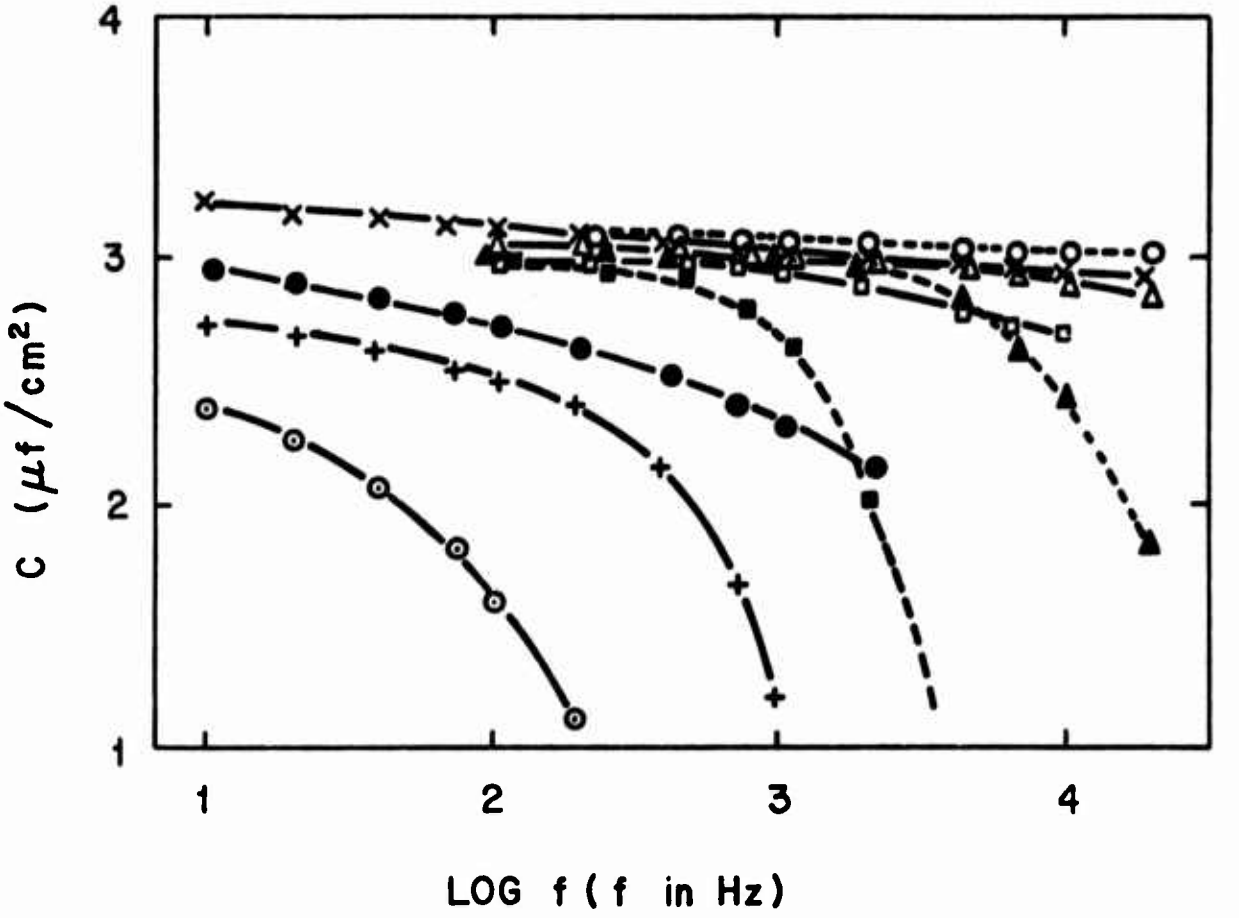

Fig. 5 Frequency dependence of capacity for the basal plane of stress-annealed pyrolytic graphite ($\Delta\theta_{\frac{1}{2}} \cong 0.4°$) in NaF solutions at 25°C and at a potential of about +0.2 V vs NHE; with hood, layer peeled off dry

x 0.9 N, square wave
o 0.9 N, sine wave
Δ 0.1 N, square wave
▲ 0.1 N, sine wave
□ 0.01 N, square wave
■ 0.01 N, sine wave
● 10^{-3} N, square wave
+ 10^{-4} N, square wave
⊙ 10^{-5} N, square wave

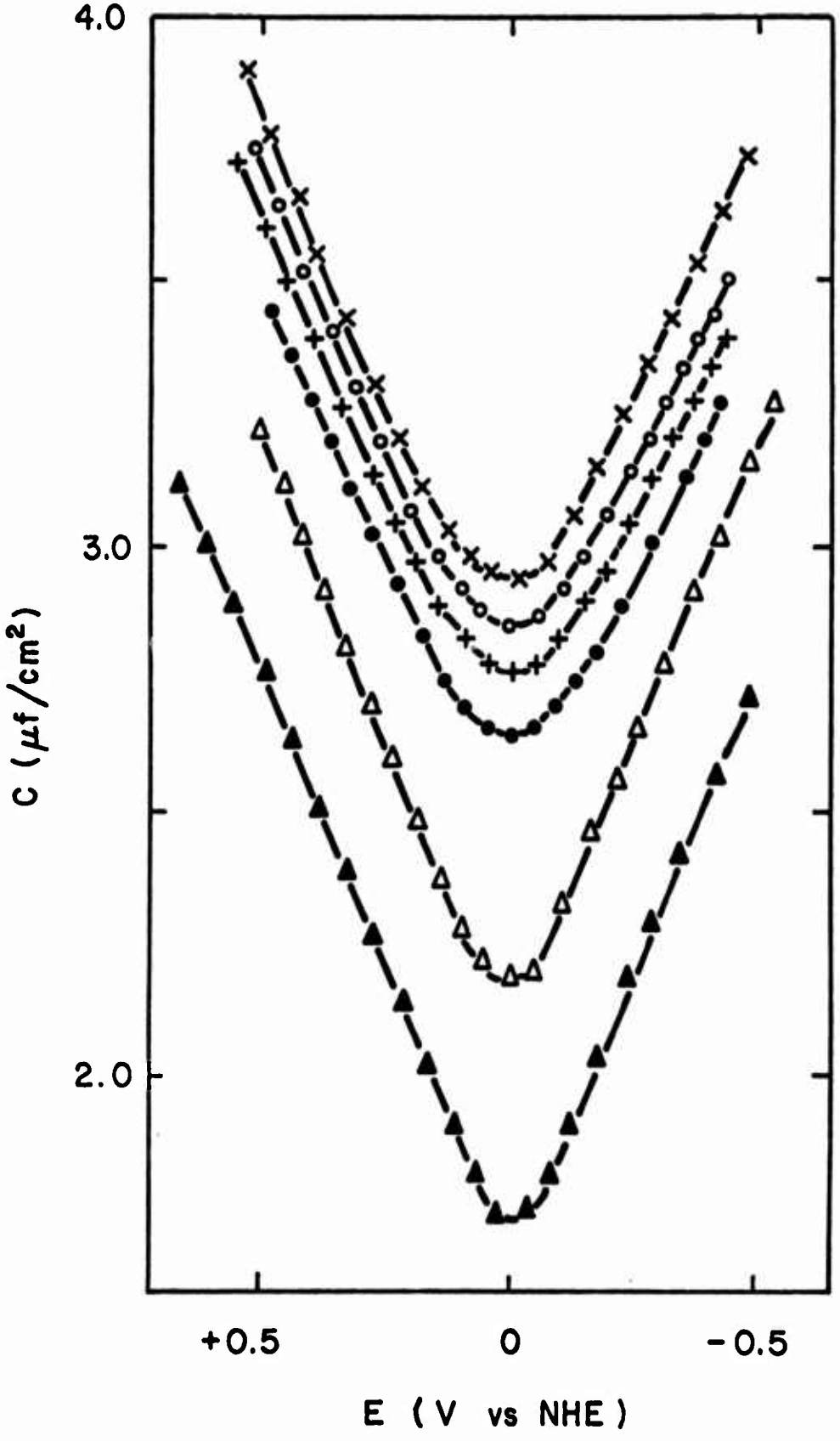

Fig. 6 Capacity-potential curves for the basal plane of stress-annealed pyrolytic graphite ($\Delta\theta_{\frac{1}{2}} \cong 0.4°$) in NaF solutions (pH ≈ 6) at 25°C and 20Hz, with hood, layer peeled off dry

x 0.9 N;
o 10^{-1} N;
+ 10^{-2} N;
• 10^{-3} N;
Δ 10^{-4} N;
▲ 10^{-5} N;

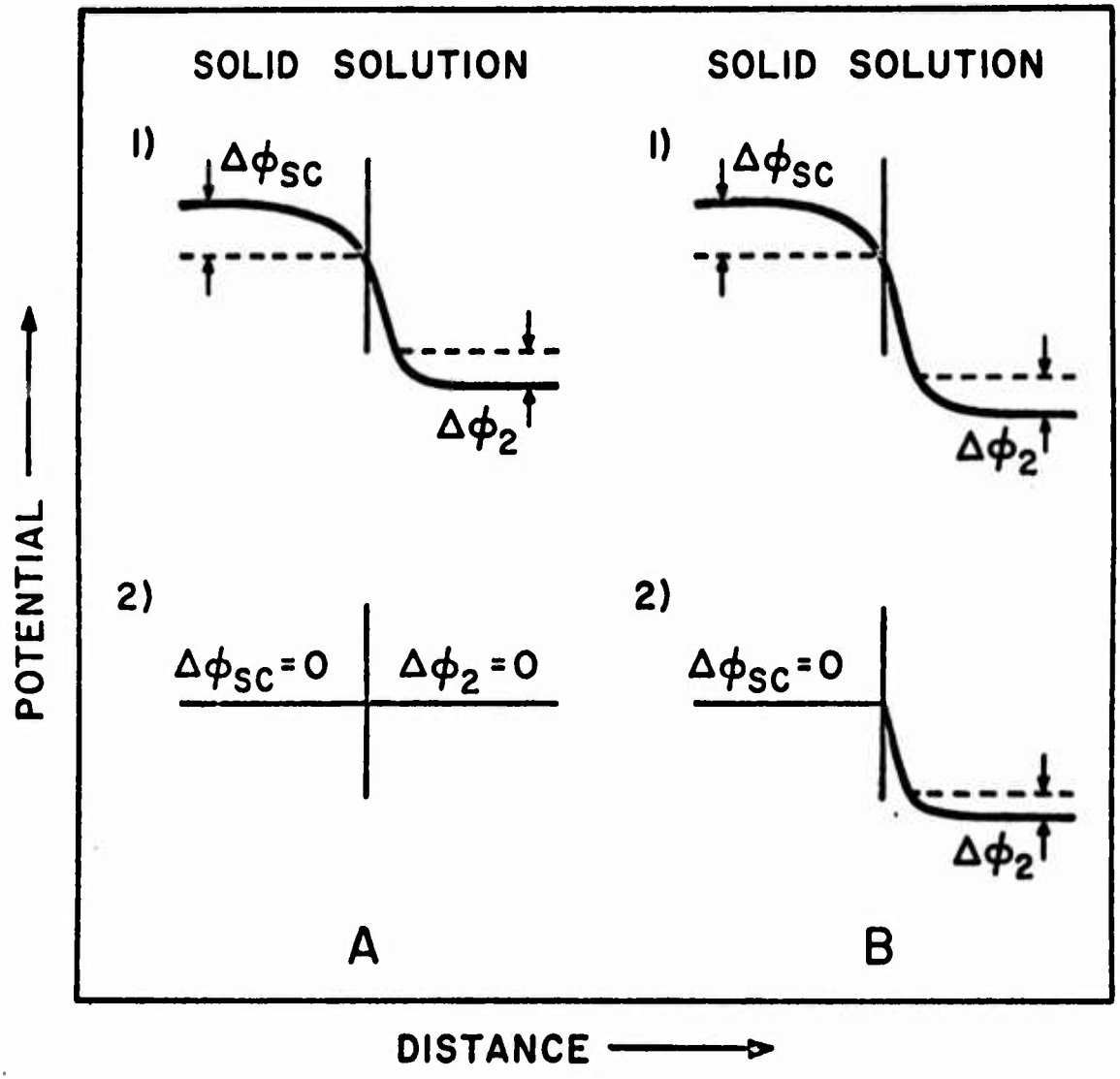

Fig. 7 Schematic representation of potential distribution at the basal plane of the pyrolytic graphite/electrolyte interface (dilute solution)

A) without appreciable contribution from surface states:

1) general case
2) at the flat band potential = point of zero charge

B) with contribution from surface states:

1) general case
2) at the flat band potential, $\Delta\phi_{sc} = 0$

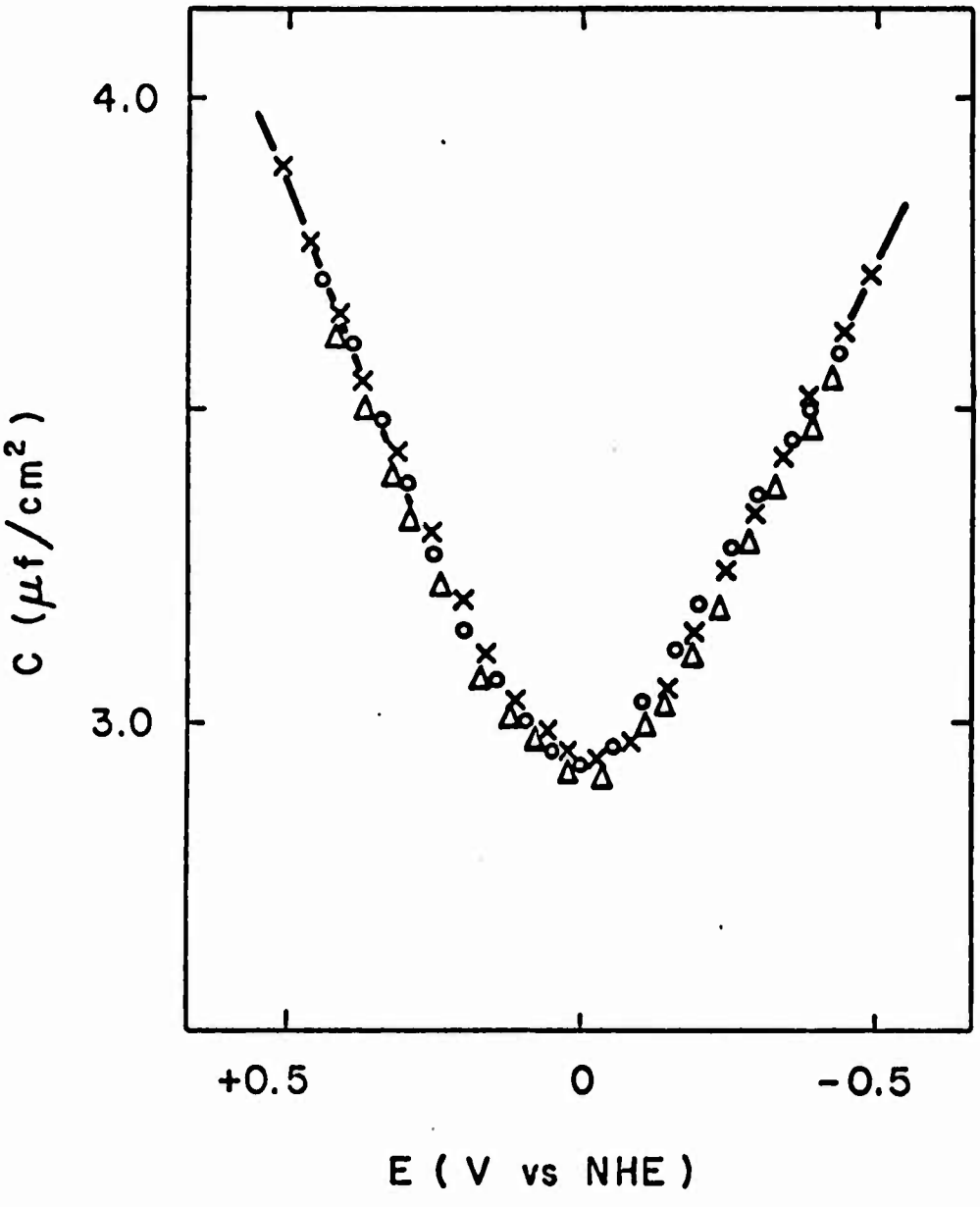

Fig. 8 Capacity-potential curves for the basal plane of stress-annealed pyrolytic graphite ($\Delta\theta_{\frac{1}{2}} \cong 0.4°$) in NaF + NaI solutions (pH ≈ 6) at 25°C and 1000 Hz (sine wave), with hood, layer peeled off dry

x 0.9 N NaF
o 0.8 N NaF + 0.1 N NaI
Δ 0.9 N NaF + 0.01 N NaI

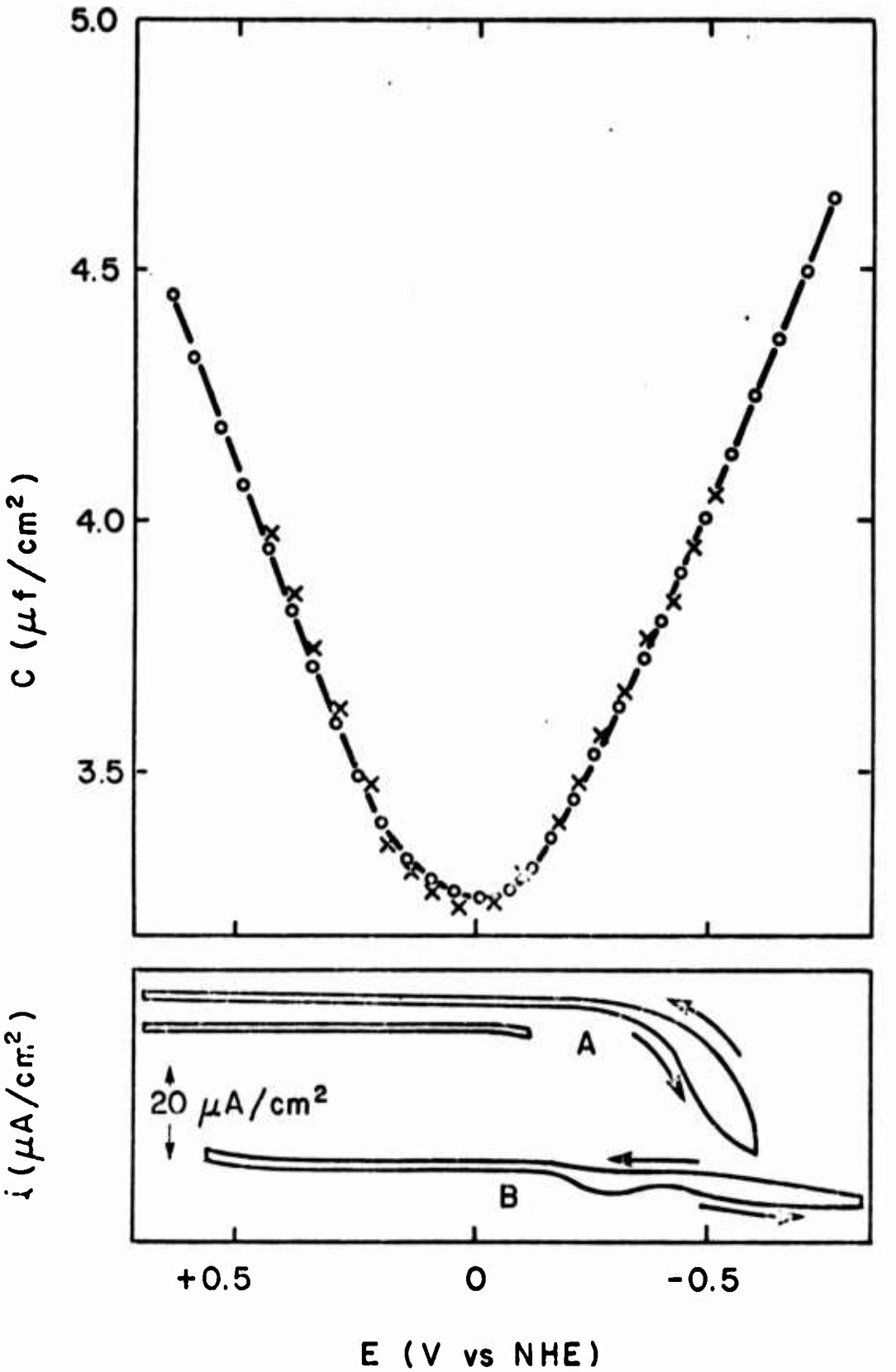

Fig. 9 Capacity-potential and current-potential curves for the basal plane of stress-annealed pyrolytic graphite ($\Delta\theta_{\frac{1}{2}} \cong 0.4°$) in 1 N H_2SO_4 and 1 N NaOH solutions at 25°C and 1000 Hz (sine wave), with hood layer peeled off dry: x 1 N H_2SO_4; o 1 N NaOH
Scan rate for the current-potential curves 0.1 V/sec, direction of sweep indicated by arrows: A) 1 N H_2SO_4; B) 1 N NaOH

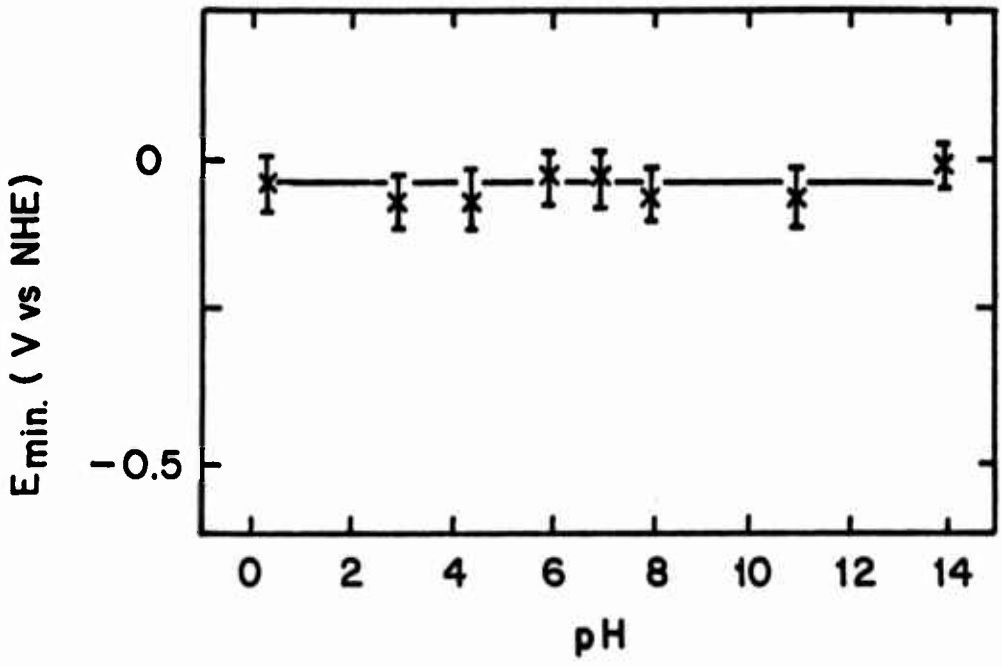

Fig. 10 pH dependence of the electrode potential for the minimum capacity for the basal plane of stress-annealed pyrolytic graphite ($\Delta\theta_{\frac{1}{2}} \cong 0.4°$) at 25°C

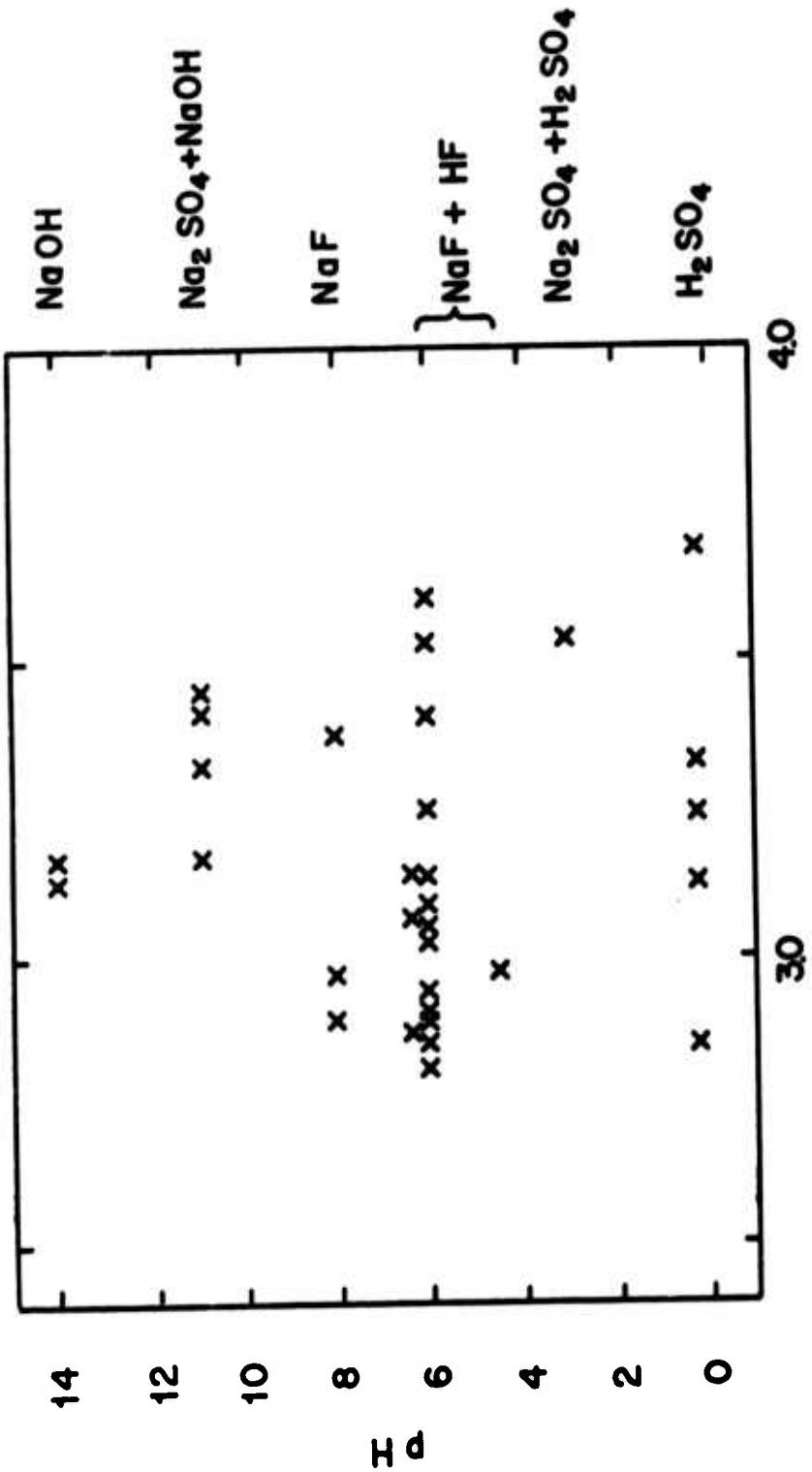

Fig. 11 pH dependence of the minimum capacity for the basal plane of stress-annealed pyrolytic graphite ($\Delta\theta_{\frac{1}{2}} = 0.4°$) at 25°C. (Each point corresponds to a new surface, prepared by the peeling technique.)

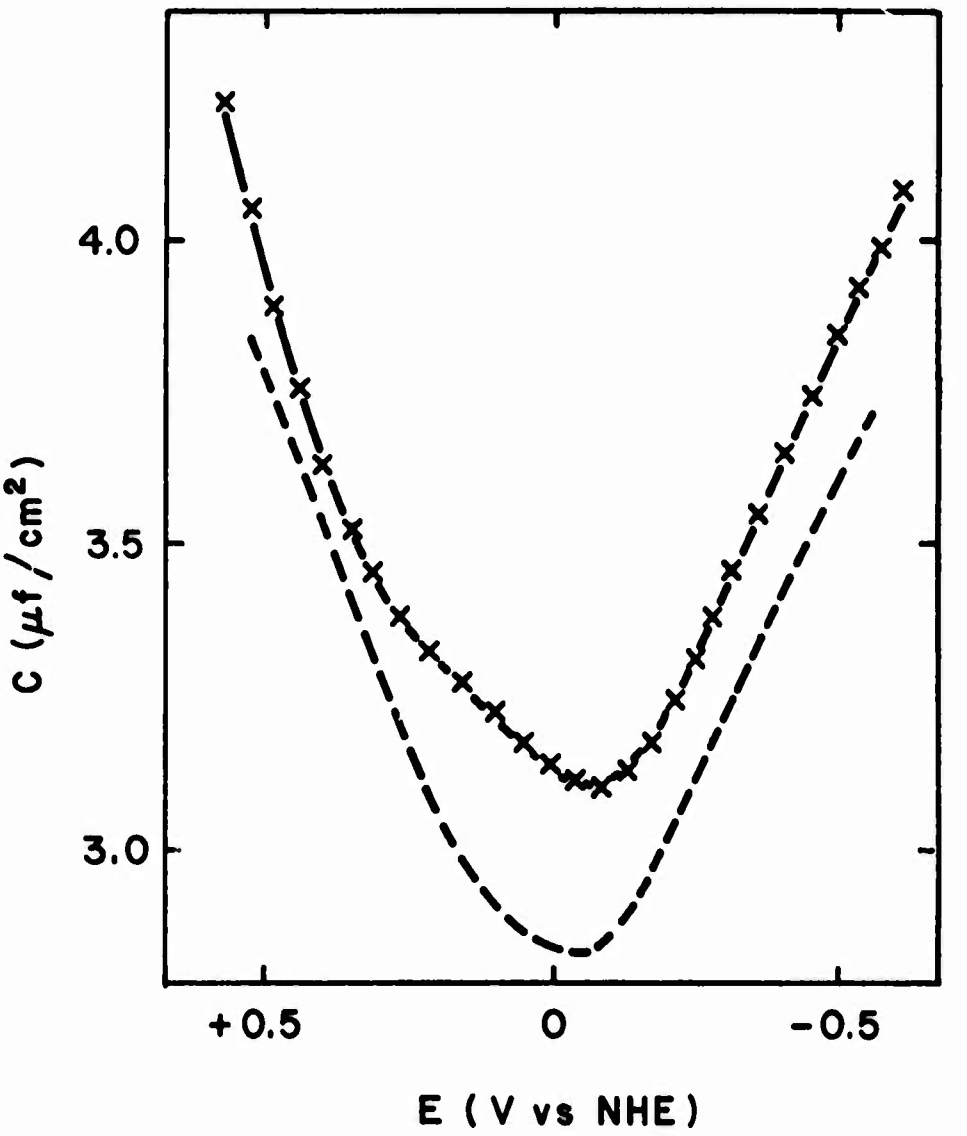

Fig. 12 Capacity-potential curves for the basal plane of annealed pyrolytic graphite with $\Delta\theta_{\frac{1}{2}} \cong 8°$, in 0.9 N NaF (pH = 6) at 25°C and 1000 Hz (sine wave), with hood, layer peeled off under electrolyte

x experimental points for annealed pyrolytic graphite with $\Delta\theta_{\frac{1}{2}} \cong 8°$

---- comparison curve for the stress-annealed pyrolytic graphite with $\Delta\theta_{\frac{1}{2}} \cong 0.4°$

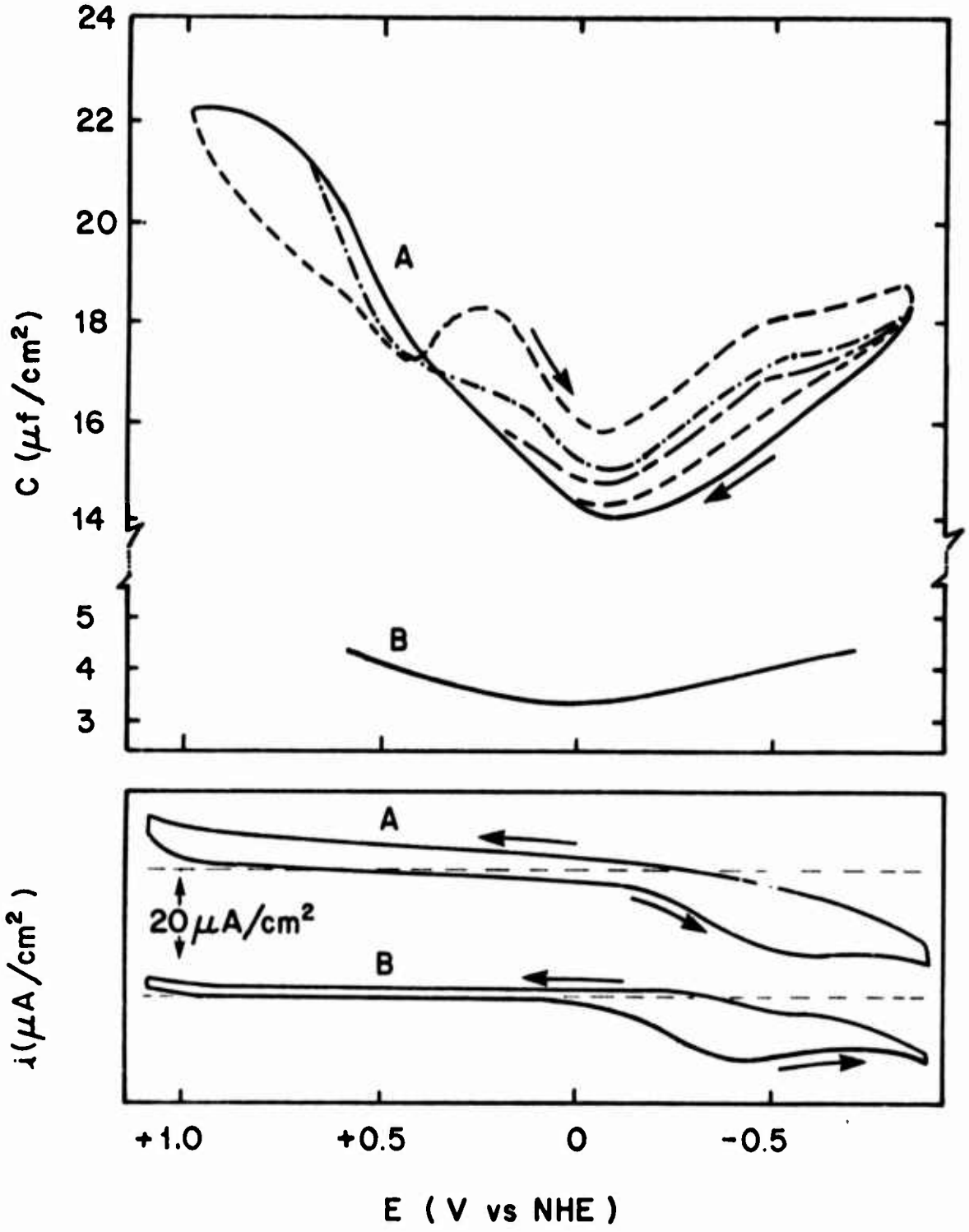

Fig. 13 Capacity-potential and current-potential curves for the basal plane of annealed pyrolytic graphite ($\Delta\theta_{\frac{1}{2}} \leq 8°$) in 0.9 N NaF (pH = 6) at 25°C and 1000 Hz (sine wave) with hood. Scan rate for the current-potential curves 0.1 V/sec; direction of sweep indicated by arrows

A) surface renewed by polishing
- _____ potentials scanning positive from -0.8 V vs NHE
- - - - potentials scanning negative from 0.1 V vs NHE
- — — — potentials scanning negative from 0.4 V vs NHE
- —.—.— potentials scanning negative from 0.7 V vs NHE
- - - - potentials scanning negative from 1.0 V vs NHE

B) Surface renewed by peeling off a layer.

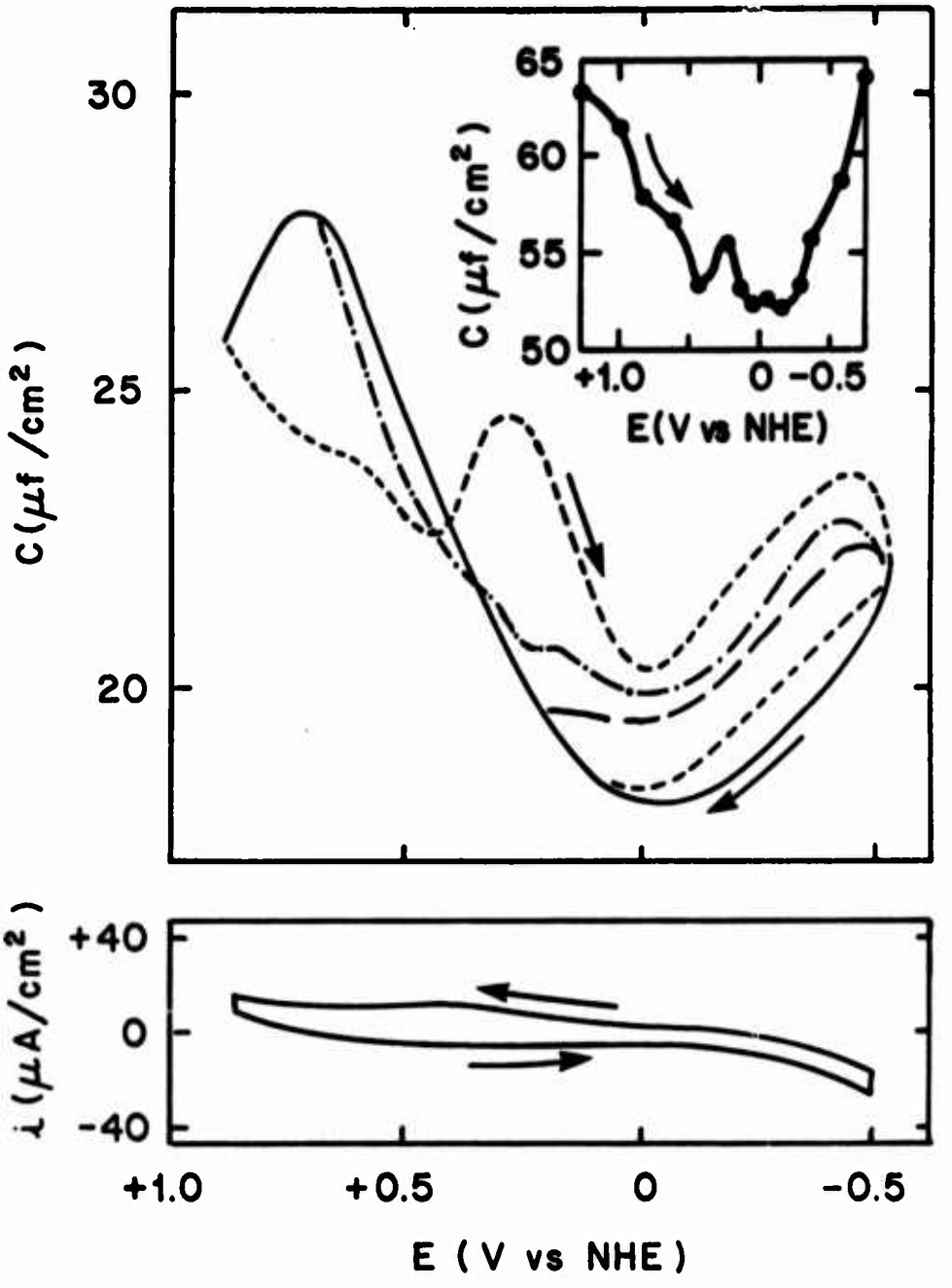

Fig. 14 Capacity-potential and current potential curves for the basal plane of ordinary pyrolytic graphite ($\Delta\theta_{\frac{1}{2}} \approx 40°$) in 0.9 N NaF (pH ≈ 6) at 25°C and 1000 Hz (sine wave), with hood, surface renewed by polishing Scan rate for the current-potential curves 0.1 V/sec, direction of sweep indicated by arrows

——— potentials scanning positive from -0.5 V vs NHE
- - - - - potentials scanning negative from 0.1 V vs NHE
— — — potentials scanning negative from 0.4 V vs NHE
—·—·— potentials scanning negative from 0.7 V vs NHE
- - - - - potentials scanning negative from 0.9 V vs NHE

Insert figure: Bauer, Sptritzer and Elving (9) data in 0.5 N KCl, resurfaced by polishing, frequency 1000 Hz.

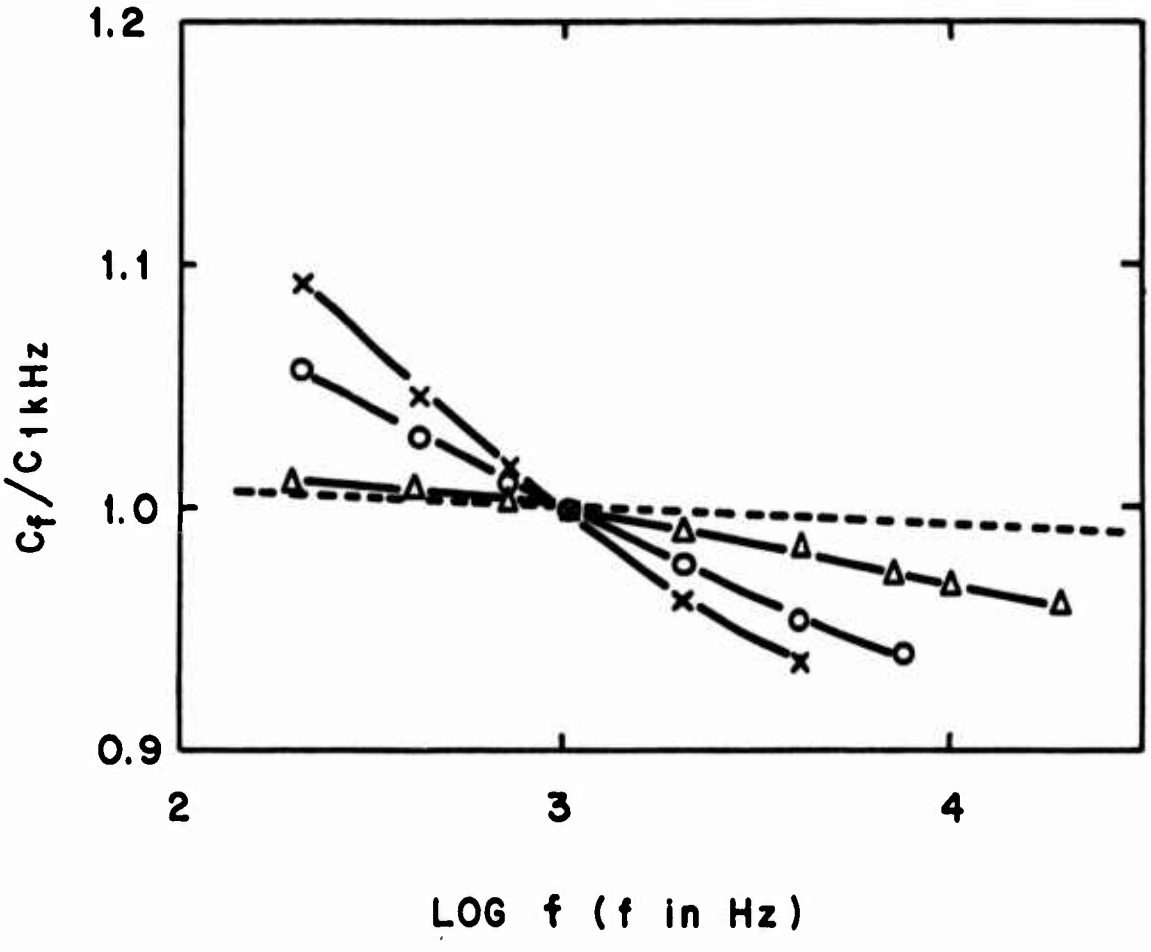

Fig. 15 Frequency dependence of capacity for the basal plane of pyrolytic graphite with different crystalline perfections in 0.9 N NaF at 25°C, with the sine wave method, with hood

x ordinary pyrolytic graphite ($\Delta\theta_{\frac{1}{2}} \approx 40°$), polished
o annealed pyrolytic graphite ($\Delta\theta_{\frac{1}{2}} \approx 8°$), polished
Δ annealed pyrolytic graphite ($\Delta\theta_{\frac{1}{2}} \approx 8°$), layer peeled off dry
- - - - stress-annealed pyrolytic graphite ($\Delta\theta_{\frac{1}{2}} \approx 0.4°$), layer peeled off dry.